Frequency-Modulated Microwave Photonic Links with Direct Detection: Review and Theory

John Wyrwas
Ming C. Wu, Ed.

Electrical Engineering and Computer Sciences
University of California at Berkeley

Technical Report No. UCB/EECS-2010-156
http://www.eecs.berkeley.edu/Pubs/TechRpts/2010/EECS-2010-156.html

December 15, 2010

Copyright © 2010, by the author(s).
All rights reserved.

Permission to make digital or hard copies of all or part of this work for personal or classroom use is granted without fee provided that copies are not made or distributed for profit or commercial advantage and that copies bear this notice and the full citation on the first page. To copy otherwise, to republish, to post on servers or to redistribute to lists, requires prior specific permission.

Acknowledgement

This work is supported by a grant from the Defense Advanced Research Projects Agency.

Frequency-Modulated Microwave Photonic Links with Direct Detection: Review and Theory

John M. Wyrwas

September 10, 2010

Abstract

This work is a theoretical study of microwave photonic links which use optical frequency modulation (FM) and filter-slope discrimination for demodulation. The high modulation efficiency of optical FM devices is attractive for achieving low noise-figure links, but linear demodulation of the signals is also desired. In order to design discriminators which produce low distortion, this paper presents general full-signal and small-signal models of the effects of arbitrary optical filtering on an FM link, including the interaction between FM and residual IM. The small signal model is used to derive figures of merit for the linearity, noise and dynamic range of the FM links. The results of the models invalidate a common assumption: that linear FM to IM discrimination is possible. Instead, the discrimination must be from FM to amplitude modulation of the electric field for the link response to be linear.

The linearity of links using two different sets of FIR discriminator filters, designed using the minimax relative error and maximally linear criteria, are compared in order to evaluate the better design method. The evolution of link linearity with filter order is studied. The analytical models are compared to numerical simulations of the filters, and the models are found to be consistent. Finally, a Monte Carlo simulation is used to analyze the sensivity to errors in fabrication for high-order filters realized in planar lightwave circuits (PLC) with a lattice filter architecture.

Contents

List of Figures

List of Tables

Chapter 1

Introduction

1.1 Microwave photonic links

Microwave photonics is the application of photonic devices, such as lasers, to microwave systems for signal generation, signal transmission and signal processing. Microwave photonic systems are analog in the sense that they manipulate arbitrary baseband signals as well as digital signals that are modulated onto a higher carrier frequency. Microwave photonic links are fiber optic links which transmit microwave signals to remote locations.

Microwave photonic links have been explored for replacing traditional coaxial links in a variety of applications because of their advantages in size, weight, immunity to electromagnetic interference, bandwidth and power consumption [1, 2, 3]. The most successful commercial applications have been in hybrid-fiber-coax (HFC) infrastructure for distributing cable-television signals and in hybrid-fiber-radio (HFR) for distributing cellular signals to remote antennas [1, 4]. Military radar and communication systems also use analog fiber optic systems for antenna remoting.

The applications of microwave photonic links are limited by the noise and distortion performance required to receive the transmitted signals. The most common

microwave photonic links are intensity-modulation direct-detection links (IM-DD), where the optical power is varied in proportion to the input signal, transmitted over optical fiber and finally directly-detected by a photodetector. The noise and distortion performance of these links, as reviewed by [5], are not yet competitive with electronic systems and are unsuitable for next generation military wireless systems. IM-DD links have high (-30 dB to -20 dB) RF-to-RF signal loss due to low modulation efficiency, which contributes greatly to poor noise figures. This provides an impetus to study other link architectures.

1.2 Frequency modulation

Modulation is not limited to the intensity, as other parameters of the light can be used to convey information. The amplitude, phase, frequency and polarization of the light's electric field are some of these quantities that can be modulated. Frequency modulated (FM) links, where the instaneous optical frequency of the laser is varied with the input signal, are considered to be promising alternatives to IM links. Directly modulated FM lasers have been demonstrated with high modulation efficiency and with modulation bandwidths that are not limited by the laser relaxation frequency [6]. Recent work on multi-section DFB [7] and EML lasers [8] have produced modulation efficiencies two orders of magnitude better than traditional intensity modulation. An improvement in modulation efficiency could make an major impact on the noise performance of microwave photonic links.

1.3 FM discriminators

Because photodetectors respond to the intensity envelope of the light and not the instantaneous frequency, a number of approaches have been developed to demodulate the FM at the output of the link. These include homodyne detection, heterodyne de-

tection and discriminator (or slope) detection. The first two systems are considered coherent detection systems, since two beams are combined coherently at the photodetector. In the third approach, an optical filter acts as an FM discriminator that converts FM to amplitude modulation (AM), and the AM is directly detected by the photodetector. Following the nomenclature of [9], such a system with a discriminator is termed an FM direct-detection (FM-DD) link. The analysis of FM-DD links is the main focus of this work.

FM-DD links use optical filters as discriminators to convert FM to AM. Paraphrasing [10], the sidebands of a frequency-modulated signal possess certain amplitude and phase relationships among themselves such that the envelope of the signal is independent of time. A discriminator works by modifying these phase and amplitude relationships such that the amplitude of the envelope of the resultant signal fluctuates in the same manner versus time as did the instantaneous frequency of the original signal.

Heuristically, one can think of the FM discriminator as a function with a frequency dependent amplitude. The slope of the function converts variations in the optical frequency into variations in the amplitude. This view is accurate for slow variations of the optical frequency. However, it can generally be misleading since it assumes that the instantaneous frequency of the light is equivalent to a time-averaged frequency. Nevertheless, the model is instructive as it suggests that functions with larger slopes will have better conversion efficiency from FM to AM, and that a function with many large high order derivatives will distort the AM signal more than one with a more "linear" function.

The optical filter used as an FM discriminator impacts the performance of the FM-DD link. The gain of the link is affected by the discriminator's conversion efficiency from FM to AM. The distortion of the link is limited by the linearity of the conversion process. Because of the long coherence lengths of lasers used in communi-

cation systems, practical filters are coherent and are appropriately analyzed as filters of light's electric field amplitude and phase, rather than as filters of the light's intensity. In this work, I derive guidelines for designing discriminator filters to ensure low signal distortion. A filter with perfectly linear phase and whose electric field transmission ramps linearly with frequency will linearly convert FM to AM. Because the signal is AM rather than IM, the photodetection process will create second-harmonics of the signal's Fourier-frequency components. This can be dealt with by a balancing approach. I also find that directly converting from FM to IM cannot be performed in a linear fashion.

1.4 Development of FM discriminators

Mach-Zehnder interferometers (MZI) were first suggested as FM discriminators, but they create large amounts of signal distortion. Alternatives to MZIs have been proposed, including Fabry-Perot interferometers, fiber Bragg gratings (FBGs) and ring resonators.

The work of Harris, [11], was the earliest use of a quadrature biased Mach Zehnder interferometer structure to discriminate optical FM. An interferometric path difference was created by passing the light through a birefringent crystal when the light's polarization was angled between the fast and slow axes of the crystal. It was noted that optimal FM to AM conversion occurs at the quadrature bias point. The technique was also applied to phase modulated light in [10]. Besides PM to AM discrimination, suppression of unwanted incident AM was done by applying a 180 degree phase shift to one of the two complementary polarization states at the output of the discriminator. The initial AM canceled when both polarization states, now with their PM in phase but AM 180 degrees out of phase, were detected at a single polarization-insensitive photodetector.

The authors understood that linear demodulation, required for high fidelity signal transmission, could be accomplished with a discriminator that has a linear FM to AM transfer function, and that high-order filters could be used to implement this linear-field discriminator. In [12], they proposed a linear-field discriminator using a network of birefringent crystals. The device was a tenth-order finite-impulse-response (FIR) filter. The series of crystals worked as a series of cascaded Mach Zehnder interferometers, and the network was equivalent to a lattice filter architecture. The filter coefficients chosen were the exponential Fourier series approximation to a triangular wave.

Another physical implementation of the MZI style discriminator using mirrors and beam splitters was suggested by [13]. In this case, balanced photodetection was used to cancel AM. Such an interferometer was experimentally verified by [14]. [13] also suggested the use of balanced detection for the birefringent crystal device of [11].

Concurrent to the development of direct frequency modulation of semiconductor lasers in works such as [15], [16] performed digital data transmission experiments using a Michelson interferometer to discriminate optical frequency shift keying (FSK).

The use of FM semiconductor lasers and discriminator detection was extended to transmitting subcarrier-multiplexed, analog signals for applications in cable television distribution. Experimental results for a Fabry-Perot discriminated, FM subcarrier-multiplexed system were presented by [17]. An array of optical frequency modulated DFB lasers and a Fabry-Perot discriminator were used to transmit and demodulate a large number of microwave FM, analog video channels. A similar system was also used to transmit subcarrier-multiplexed, digital signals in [18].

Because analog links require high linearity and low noise, a number of authors have derived figures of merit for the performance of analog FM-DD links. [19] analyzed the frequency-dependent response of a link with a quadrature biased MZI discriminator subject to large modulation-depth AM and FM. [20] studied the intermodulation

distortion for a Fabry-Perot discriminated link with a large number of channels, while taking into account both FM and IM on each channel. [21] derived figures of merit for the dynamic range of a phase modulated link with an MZI discriminator and balanced detection.

[22] studied a link with an arbitrary discriminator. The general formulae were applied to the particular cases of an MZI and a Fabry-Perot interferometer. However, the analysis was inaccurate since it looked at the system in terms of light intensity transmission through the interferometer. The transmission was expanded in terms of a Taylor series. The analysis assumed that derivatives of the transmission spectrum of the interferometer (in the Fourier-frequency domain) with respect to the instantaneous optical frequency were proportional to overall link nonlinearity. Similar (inaccurate) theoretical analyses using Taylor series were published by [23] and [24]. However, these papers did include new models for the nonlinearities in the lasers' FM and included the effects of residual IM.

To improve the linearity of an FM-DD link, many alternatives to the Mach-Zehnder and Fabry-Perot interferometers have been suggested. Except for the early work of [12], all of these "linearized" discriminators were designed such that the filter's optical intensity transmission was linear with frequency, rather than the field amplitude. [25] and [26] proposed pairs of chirped fiber-Bragg gratings with either the index variation or chirp rate varied nonlinearly. [27] proposed a frequency discriminator based on an MZI with ring resonators in its arms. [28] suggested that the linearity of a Sagnac discriminator could be improved by adding ring resonators.

Experimental and theoretical results using fiber-Bragg gratings were presented in [29, 30, 31, 32, 33, 34]. These experiments used pairs of complementary gratings designed to have linear intensity. The gratings were low-biased to perform carrier suppression. In [31, 33], the authors presented a clipping-free dynamic range limit for an FM-DD system. (In related work, [35, 36], the authors used Bragg gratings

to convert phase modulation into single sideband modulation.) The authors later realized that linear FM to IM discrimination was not consistent with their theoretical analysis, [32]:

> [...] the ideal linear power reflectivity-versus-frequency curve does not result in an ideal half-wave rectification, as suggested by the simple time-domain view. Rather, in addition to the signal component, the output includes a dc component as well as a nonlinear distortion.

They explained the discrepancy, [34]:

> The reason this intuition fails is that combining a time-domain view of the FM signal (instantaneous frequency, not averaged over time) with a frequency domain view of the FBG filter response is inconsistent with the frequency domain analysis [...]

It is erroneous to think of the modulated signal in terms of its instantaneous frequency while looking at the frequency spectrum of the filter. The carrier is not really being swept along the ramp of the filter by the modulation, so analyzing it in the same way as, for example, the small-signal current to voltage relationship of an amplifier is not correct. In this work, I present FM to AM discrimination as an alternative which can produce a microwave photonic link with low distortion. The following chapter analytically demonstrates this result.

Chapter 2

Analytical link analysis

In this chapter, I derive figures-of-merit for an FM-DD link that uses an arbitrary optical filter for discrimination [37]. I find expressions for the currents at each microwave frequency at the output of the link under a two-tone test. I take a small-modulation-depth approximation and obtain expressions for the signal-to-noise ration (SNR), second-order and third-order output intercept points (OIP2 and OIP3), spurious-free dynamic range (SFDR) and noise figure (NF). I apply these general formulae to the specific cases of the Mach Zehnder interferometer, a linear-intensity filter and a linear-field filter. The analysis of the MZI is consistent with earlier theory. I show that the linear-intensity filter does not convert FM to IM in a linear fashion, but the linear-field filter actually does convert FM to AM in a linear fashion. For the linear-field filter, I derive the noise figure's dependence on the link's regime of operation and quantify the effect of the laser's residual IM on the distortion.

2.1 Response of filtered FM link

In this section, I derive expressions for the rf photocurrents produced at the output of an FM-DD link with an arbitrary filter. An FM-DD link consists of an FM laser, an optical filter and a photodetector. The source's residual IM and the filter's

nonlinearities are the main constributions to distortion on the link. To quantify the nonlinearities, I apply a two-tone distortion test. An optical signal that is phase or frequency modulated by two sinusoidal tones can be represented by the time varying electric field

$$e(t) = \kappa\sqrt{2P_{opt}}\cos\left[2\pi f_c t + \beta_1 \sin(2\pi f_1 t) + \beta_2 \sin(2\pi f_2 t)\right] \tag{2.1.1}$$

where P_{opt} is the rms optical power, κ is a constant relating optical field and optical power such that $P_{opt} = \left\langle e(t)^2 \right\rangle / \kappa^2$, f_c is the frequency of the optical carrier, f_1 and f_2 are the modulation frequencies and β_1 and β_2 are the angle modulation depths. For FM, each modulation depth is equal to the maximum optical frequency deviation of the carrier induced by the modulation divided by the frequency of the modulation, $\beta = \delta_f / f$. The modulation of the light can be thought of in terms of variations in the instantaneous frequency of the light due to the applied signal. The optical frequency, or wavelength, varies sinusoidally in time. The instantaneous frequency of the light is given by the derivative of the phase of the light,

$$\frac{1}{2\pi}\frac{\partial}{\partial t}\left[2\pi f_c t + \beta_1 \sin(2\pi f_1 t) + \beta_2 \sin(2\pi f_2 t)\right] = f_c + \delta_{f_1}\cos(2\pi f_1 t) + \delta_{f_2}\cos(2\pi f_2 t) \tag{2.1.2}$$

An FM laser is non-ideal as it produces undesired residual IM and includes noise. The correction to the electric field is

$$\begin{aligned} e(t) =& a(t) + \kappa\sqrt{2P_{opt}\left[1 + n(t)\right]} \\ &\cdot \sqrt{1 + m_1\cos(2\pi f_1 t + \phi) + m_2\cos(2\pi f_2 t + \phi)} \\ &\cdot \cos\left[2\pi f_c t + \beta_1 \sin(2\pi f_1 t) + \beta_2 \sin(2\pi f_2 t) + \varphi(t)\right] \end{aligned} \tag{2.1.3}$$

where $n(t)$ is the RIN of the source, $\varphi(t)$ is the phase noise of the source, $a(t)$ is the

ASE noise from an optical amplifier, m_1 and m_2 represent the IM depths for the two tones and ϕ is the phase difference between the IM and the FM. The link will also amplify thermal noise present at the input.

An arbitrary optical filter is used on the link to convert FM to IM. Using the Jacobi-Anger expansion, the electric field after the filter can be expressed as an infinited weighted sum over sidebands. I employ a shorthand notation to describe the electric field transmission at each frequency in the optical spectrum that corresponds to an optical sideband,

$$h_{n,p} \equiv h\left(f = f_c + nf_1 + pf_2\right) \tag{2.1.4}$$

where n and p are integer indices and h is the complex transfer function of the filter, representing its phase and amplitude response, including any insertion losses or optical amplifier gain. For example, $h_{0,0}$ is the field transmission for the optical carrier, and $h_{-1,0}$ is the transmission of the negative, first order sideband spaced f_1 away from the carrier.

After the filter, the light is incident upon a photodetector. I derive the output current from the photodetector and approximate it for small modulation depth. The standard definitions for the linearity figures of merit rely on this approximation. The residual IM depth and the intensity noise are assumed to be much smaller than the FM, so the square root in (2.1.3) can be expanded using a Taylor series, yielding

$$\begin{aligned} e\left(t\right) \approx & a\left(t\right) + \kappa\sqrt{2P_{opt}} \\ & \cdot \left(1 + \frac{1}{2}m_1 \cos\left(2\pi f_1 t + \phi\right) + \frac{1}{2}m_2 \cos\left(2\pi f_2 t + \phi\right) + \frac{1}{2}n\left(t\right)\right) \\ & \cdot \cos\left[2\pi f_c t + \beta_1 \sin\left(2\pi f_1 t\right) + \beta_2 \sin\left(2\pi f_2 t\right) + \varphi(t)\right] \end{aligned} \tag{2.1.5}$$

Ignoring noise, this can be written using an angular addition trigonometric identity

as

$$
\begin{aligned}
e\left(t\right) = \kappa\sqrt{2P_{opt}}Re\Big\{ & \\
& \cos\left[2\pi f_c t + \beta_1 \sin\left(2\pi f_1 t\right) + \beta_2 \sin\left(2\pi f_2 t\right)\right] \\
& + \frac{1}{4} m_1 \cos\left[2\pi\left(f_c + f_1\right) t + \beta_1 \sin\left(2\pi f_1 t\right) + \beta_2 \sin\left(2\pi f_2 t\right) + \phi\right] \\
& + \frac{1}{4} m_1 \cos\left[2\pi\left(f_c - f_1\right) t + \beta_1 \sin\left(2\pi f_1 t\right) + \beta_2 \sin\left(2\pi f_2 t\right) - \phi\right] \\
& + \frac{1}{4} m_2 \cos\left[2\pi\left(f_c + f_2\right) t + \beta_1 \sin\left(2\pi f_1 t\right) + \beta_2 \sin\left(2\pi f_2 t\right) + \phi\right] \\
& + \frac{1}{4} m_2 \cos\left[2\pi\left(f_c - f_1\right) t + \beta_1 \sin\left(2\pi f_1 t\right) + \beta_2 \sin\left(2\pi f_2 t\right) - \phi\right] \Big\}
\end{aligned}
$$

The Jacobi-Anger expansion is given by $e^{izcos\theta} = \sum_{n=-\infty}^{\infty} j^n J_n\left(z\right) e^{in\theta}$, where j is the imaginary unit and $J_n(z)$ is a Bessel function of the first kind. Applying this formula, the expression expands to

$$
\begin{aligned}
e\left(t\right) = \kappa\sqrt{2P_{opt}}Re\Big\{ & \\
& \sum_{n=-\infty}^{\infty} \sum_{p=-\infty}^{\infty} J_n\left(\beta_1\right) J_p\left(\beta_2\right) \exp\left[j2\pi\left(f_c + nf_1 + pf_2\right) t\right] \\
& + \frac{1}{4} m_1 \sum_{n=-\infty}^{\infty} \sum_{p=-\infty}^{\infty} J_n\left(\beta_1\right) J_p\left(\beta_2\right) \exp\left[j2\pi\left(f_c + [n+1] f_1 + pf_2\right) t + j\phi\right] \\
& + \frac{1}{4} m_1 \sum_{n=-\infty}^{\infty} \sum_{p=-\infty}^{\infty} J_n\left(\beta_1\right) J_p\left(\beta_2\right) \exp\left[j2\pi\left(f_c + [n-1] f_1 + pf_2\right) t - j\phi\right] \\
& + \frac{1}{4} m_2 \sum_{n=-\infty}^{\infty} \sum_{p=-\infty}^{\infty} J_n\left(\beta_1\right) J_p\left(\beta_2\right) \exp\left[j2\pi\left(f_c + nf_1 + [p+1] f_2\right) t + j\phi\right] \\
& + \frac{1}{4} m_2 \sum_{n=-\infty}^{\infty} \sum_{p=-\infty}^{\infty} J_n\left(\beta_1\right) J_p\left(\beta_2\right) \exp\left[j2\pi\left(f_c + nf_1 + [p-1] f_2\right) t - j\phi\right] \Big\}
\end{aligned}
$$

The signal passes through the FM discriminator filter. The electric field after the

filter is

$$
\begin{aligned}
e(t) = \kappa\sqrt{2P_{opt}}Re\Big\{ & \\
& \sum_{n=-\infty}^{\infty}\sum_{p=-\infty}^{\infty} J_n(\beta_1) J_p(\beta_2) h_{n,p} \exp\left[j2\pi\left(f_c + nf_1 + pf_2\right)t\right] \\
& + \frac{1}{4}m_1 \sum_{n=-\infty}^{\infty}\sum_{p=-\infty}^{\infty} J_n(\beta_1) J_p(\beta_2) h_{n+1,p} \exp\left[j2\pi\left(f_c + [n+1]f_1 + pf_2\right)t + j\phi\right] \\
& + \frac{1}{4}m_1 \sum_{n=-\infty}^{\infty}\sum_{p=-\infty}^{\infty} J_n(\beta_1) J_p(\beta_2) h_{n-1,p} \exp\left[j2\pi\left(f_c + [n-1]f_1 + pf_2\right)t - j\phi\right] \\
& + \frac{1}{4}m_2 \sum_{n=-\infty}^{\infty}\sum_{p=-\infty}^{\infty} J_n(\beta_1) J_p(\beta_2) h_{n,p+1} \exp\left[j2\pi\left(f_c + nf_1 + [p+1]f_2\right)t + j\phi\right] \\
& + \frac{1}{4}m_2 \sum_{n=-\infty}^{\infty}\sum_{p=-\infty}^{\infty} J_n(\beta_1) J_p(\beta_2) h_{n,p-1} \exp\left[j2\pi\left(f_c + nf_1 + [p-1]f_2\right)t - j\phi\right] \Big\}
\end{aligned}
$$

The indices of each infinite sum can be renumbered to obtain

$$
\begin{aligned}
e(t) = \kappa\sqrt{2P_{opt}}Re\Big\{ & \\
& \sum_{n=-\infty}^{\infty}\sum_{p=-\infty}^{\infty} J_n(\beta_1) J_p(\beta_2) h_{n,p} \exp\left[j2\pi\left(f_c + nf_1 + pf_2\right)t\right] \\
& + \frac{1}{4}m_1 \sum_{n=-\infty}^{\infty}\sum_{p=-\infty}^{\infty} J_{n-1}(\beta_1) J_p(\beta_2) h_{n,p} \exp\left[j2\pi\left(f_c + nf_1 + pf_2\right)t + j\phi\right] \\
& + \frac{1}{4}m_1 \sum_{n=-\infty}^{\infty}\sum_{p=-\infty}^{\infty} J_{n+1}(\beta_1) J_p(\beta_2) h_{n,p} \exp\left[j2\pi\left(f_c + nf_1 + pf_2\right)t - j\phi\right] \\
& + \frac{1}{4}m_2 \sum_{n=-\infty}^{\infty}\sum_{p=-\infty}^{\infty} J_n(\beta_1) J_{p-1}(\beta_2) h_{n,p} \exp\left[j2\pi\left(f_c + nf_1 + pf_2\right)t + j\phi\right] \\
& + \frac{1}{4}m_2 \sum_{n=-\infty}^{\infty}\sum_{p=-\infty}^{\infty} J_n(\beta_1) J_{p+1}(\beta_2) h_{n,p} \exp\left[j2\pi\left(f_c + nf_1 + pf_2\right)t - j\phi\right] \Big\}
\end{aligned}
$$

This simplifies to a compact expression for the signal after the filter in terms of its frequency components,

$$e(t) = \kappa\sqrt{2P_{opt}}Re\left\{\sum_{n=-\infty}^{\infty}\sum_{p=-\infty}^{\infty} j_{n,p}\exp\left[j2\pi\left(f_c + nf_1 + pf_2\right)t\right]\right\} \tag{2.1.6}$$

where I define

$$\begin{aligned} j_{n,p} \equiv & h_{n,p}\left\{J_n\left(\beta_1\right)J_p\left(\beta_2\right)\right. \\ & + \frac{1}{4}m_1\left[J_{n-1}\left(\beta_1\right)e^{j\phi} + J_{n+1}\left(\beta_1\right)e^{-j\phi}\right]J_p\left(\beta_2\right) \\ & \left. + \frac{1}{4}m_2 J_n\left(\beta_1\right)\left[J_{p-1}\left(\beta_2\right)e^{j\phi} + J_{p+1}\left(\beta_1\right)e^{-j\phi}\right]\right\} \end{aligned} \tag{2.1.7}$$

The electric field is incident upon a photodetector at the termination of a fiber-optic link. The photodetector is assumed to be an ideal square-law detector operating in its linear regime with responsivity $\Re$. The photocurrent is

$$i(t) = \Re P_{opt}\left\{\sum_{n=-\infty}^{\infty}\sum_{p=-\infty}^{\infty}\sum_{g=-\infty}^{\infty}\sum_{k=-\infty}^{\infty} j_{n,p}j_{g,k}^{*}\exp\left[j2\pi\left(\left[n-g\right]f_1 + \left[p-k\right]f_2\right)t\right]\right\} \tag{2.1.8}$$

This can be split up into the dc term, harmonics of f_1, harmonics of f_2 and mixtures between f_1 and f_2.

$$\begin{aligned} i(t) = & \Re P_{opt}\left\{\sum_{g=-\infty}^{\infty}\sum_{k=-\infty}^{\infty}\left|j_{g,k}\right|^2\right. \\ & + \sum_{n=-\infty}^{\infty,n\neq g}\sum_{g=-\infty}^{\infty}\sum_{k=-\infty}^{\infty} j_{n,k}j_{g,k}^{*}\exp\left[j2\pi\left[n-g\right]f_1 t\right] \\ & + \sum_{p=-\infty}^{\infty,p\neq k}\sum_{g=-\infty}^{\infty}\sum_{k=-\infty}^{\infty} j_{g,p}j_{g,k}^{*}\exp\left[j2\pi\left[p-k\right]f_2 t\right] \\ & \left. + \sum_{n=-\infty}^{\infty,n\neq g}\sum_{p=-\infty}^{\infty,p\neq k}\sum_{g=-\infty}^{\infty}\sum_{k=-\infty}^{\infty} j_{n,p}j_{g,k}^{*}\exp\left[j2\pi\left(\left[n-g\right]f_1 + \left[p-k\right]f_2\right)t\right]\right\} \end{aligned}$$

The indices of each infinite sum can be renumbered to obtain

$$
\begin{aligned}
i(t) = \Re P_{opt} \Bigg\{ & \sum_{g=-\infty}^{\infty} \sum_{k=-\infty}^{\infty} |j_{g,k}|^2 \\
& + \sum_{n=-\infty}^{\infty, n\neq 0} \sum_{g=-\infty}^{\infty} \sum_{k=-\infty}^{\infty} j_{n+g,k} j_{g,k}^* \exp\left[j2\pi n f_1 t\right] \\
& + \sum_{p=-\infty}^{\infty, p\neq 0} \sum_{g=-\infty}^{\infty} \sum_{k=-\infty}^{\infty} j_{g,p+k} j_{g,k}^* \exp\left[j2\pi p f_2 t\right] \\
& + \sum_{n=-\infty}^{\infty, n\neq 0} \sum_{p=-\infty}^{\infty, p\neq 0} \sum_{g=-\infty}^{\infty} \sum_{k=-\infty}^{\infty} j_{n+g,p+k} j_{g,k}^* \exp\left[j2\pi \left(n f_1 + p f_2\right) t\right] \Bigg\}
\end{aligned}
$$

The double infinite sums over n and p are rewritten as singly infinite sums, and the sums over negative integers have their signs flipped giving

$$
\begin{aligned}
i(t) = \Re P_{opt} \Bigg\{ & \sum_{g=-\infty}^{\infty} \sum_{k=-\infty}^{\infty} |j_{g,k}|^2 \\
& + \sum_{n=1}^{\infty} \sum_{g=-\infty}^{\infty} \sum_{k=-\infty}^{\infty} \left(j_{n+g,k} j_{g,k}^* \exp\left[j2\pi n f_1 t\right] + j_{-n+g,k} j_{g,k}^* \exp\left[-j2\pi n f_1 t\right] \right) \\
& + \sum_{p=1}^{\infty} \sum_{g=-\infty}^{\infty} \sum_{k=-\infty}^{\infty} \left(j_{g,p+k} j_{g,k}^* \exp\left[j2\pi p f_2 t\right] + j_{g,-p+k} j_{g,k}^* \exp\left[-j2\pi p f_2 t\right] \right) \\
& + \sum_{n=1}^{\infty} \sum_{p=1}^{\infty} \sum_{g=-\infty}^{\infty} \sum_{k=-\infty}^{\infty} \\
& \Big(j_{n+g,p+k} j_{g,k}^* \exp\left[j2\pi \left(n f_1 + p f_2\right) t\right] + j_{-n+g,-p+k} j_{g,k}^* \exp\left[-j2\pi \left(n f_1 + p f_2\right) t\right] \\
& + j_{n+g,-p+k} j_{g,k}^* \exp\left[j2\pi \left(n f_1 - p f_2\right) t\right] + j_{-n+g,p+k} j_{g,k}^* \exp\left[-j2\pi \left(n f_1 - p f_2\right) t\right] \Big) \Bigg\}
\end{aligned}
$$

A number added to its complex conjugate is twice the real part. With this simplification, this arranges to a final expression for the link output given an arbitrary filter:

$$
\begin{aligned}
i(t) = & \Re P_{opt} Re \left\{ \sum_{g=-\infty}^{\infty} \sum_{k=-\infty}^{\infty} |j_{g,k}|^2 \right. \\
& + 2 \sum_{n=1}^{\infty} \sum_{g=-\infty}^{\infty} \sum_{k=-\infty}^{\infty} j_{n+g,k} j_{g,k}^{*} \exp\left[j2\pi n f_1 t\right] \\
& + 2 \sum_{p=1}^{\infty} \sum_{g=-\infty}^{\infty} \sum_{k=-\infty}^{\infty} j_{g,p+k} j_{g,k}^{*} \exp\left[j2\pi p f_2 t\right] \\
& + 2 \sum_{n=1}^{\infty} \sum_{p=1}^{\infty} \sum_{g=-\infty}^{\infty} \sum_{k=-\infty}^{\infty} j_{n+g,p+k} j_{g,k}^{*} \exp\left[j2\pi \left(n f_1 + p f_2\right) t\right] \\
& \left. + 2 \sum_{n=1}^{\infty} \sum_{p=1}^{\infty} \sum_{g=-\infty}^{\infty} \sum_{k=-\infty}^{\infty} j_{n+g,-p+k} j_{g,k}^{*} \exp\left[j2\pi \left(n f_1 - p f_2\right) t\right] \right\}
\end{aligned}
\tag{2.1.9}
$$

The double-sum over indices g and k gives the contribution of each pair of optical sidebands that beat together to produce the rf photocurrent. In this form, the current is separated into different frequency components which are indicated by the summation indices n and p . The first term, where n and p are both identically zero, gives the dc. The second term, a summation over the index n, gives the fundamental tone at frequency f_1 and its harmonics. The third term, a summation over the index p, gives the fundamental tone at frequency f_2 and its harmonics. The fourth term is the sum frequencies produced by the mixing, and the fifth term is the difference frequencies produced by the mixing.

For small modulation depth, $\beta \ll 1$, and no residual IM, $m = 0$, the Bessel functions can be approximated by $J_0(z) \approx 1$ and $J_n(z) \approx (z/2)^{|n|} / |n|!$, for positive n, noting that $J_{-n}(z) = (-1)^n J_n(z)$. Keeping terms of lowest polynomial order, the current simplifies to the following equation (2.1.10). This equation gives the small

signal approximation for any frequency:

$$
\begin{aligned}
i(t) =& \Re P_{opt} Re\left\{|h_{0,0}|^2\right. \\
&+ 2\sum_{n=1}^{\infty}\sum_{g=0}^{n}\frac{\beta_1^n}{2^n}\frac{(-1)^g}{(n-g)!g!}h_{n-g,0}h_{-g,0}^{*}\exp\left[j2\pi n f_1 t\right] \\
&+ 2\sum_{p=1}^{\infty}\sum_{k=0}^{p}\frac{\beta_2^p}{2^p}\frac{(-1)^k}{(p-k)!k!}h_{0,p-k}h_{0,-k}^{*}\exp\left[j2\pi p f_2 t\right] \\
&+ 2\sum_{n=1}^{\infty}\sum_{p=1}^{\infty}\sum_{g=0}^{n}\sum_{k=0}^{p}\frac{\beta_1^n\beta_2^p}{2^{n+p}}\frac{(-1)^{g+k}}{(n-g)!g!\,(p-k)\,k!}h_{n-g,p-k}h_{-g,-k}^{*}\exp\left[j2\pi\left(nf_1+pf_2\right)t\right] \\
&\left.+2\sum_{n=1}^{\infty}\sum_{p=1}^{\infty}\sum_{g=0}^{n}\sum_{k=0}^{p}\frac{\beta_1^n\beta_2^p}{2^{n+p}}\frac{(-1)^{p+g+k}}{(n-g)!g!\,(p-k)\,k!}h_{n-g,-p+k}h_{-g,k}^{*}\exp\left[j2\pi\left(nf_1-pf_2\right)t\right]\right\}
\end{aligned}
\tag{2.1.10}
$$

There are four current components of interest. The amplitude of the dc, as should be expected, is proportional to the optical power in the optical carrier after the filter. The current at the fundamental frequency f_1 is linearly proportional to the modulation depth. It depends on the negative and positive first-order sidebands beating with the optical carrier. The current at the second-harmonic frequency $2f_1$ has a quadratic relationship to modulation depth. It depends on the second-order sidebands beating with the optical carrier, as well as the first-order sidebands beating with each other. The current produced at the difference frequency $2f_1 - f_2$ is a third-order intermodulation product. These currents are

$$i_{dc} = \Re P_{opt} X_0 \tag{2.1.11}$$

$$i_{f_1} = \Re P_{opt}\beta_1 Re\left\{X_1\exp\left[j2\pi f_1 t\right]\right\} \tag{2.1.12}$$

$$i_{2f_1} = \Re P_{opt}\frac{1}{4}\beta_1^2 Re\left\{X_2\exp\left[j4\pi f_1 t\right]\right\} \tag{2.1.13}$$

$$i_{2f_1-f_2} = \Re P_{opt}\frac{1}{8}\beta_1^2\beta_2 Re\left\{X_3\exp\left[j2\pi\left(2f_1-f_2\right)t\right]\right\} \tag{2.1.14}$$

where for convenience, I define the following complex constants

$$X_0 = h_{0,0}h^*_{0,0} \tag{2.1.15}$$

$$X_1 = h_{1,0}h^*_{0,0} - h_{0,0}h^*_{-1,0} \tag{2.1.16}$$

$$Y_1 = h_{1,0}h^*_{0,0} + h_{0,0}h^*_{-1,0} \tag{2.1.17}$$

$$X_2 = h_{2,0}h^*_{0,0} - 2h_{1,0}h^*_{-1,0} + h_{0,0}h^*_{-2,0} \tag{2.1.18}$$

$$\begin{aligned} X_3 = &- h_{2,-1}h^*_{0,0} + h_{2,0}h^*_{0,1} + 2h_{1,-1}h^*_{-1,0} \\ &+ h_{0,0}h^*_{-2,1} - h_{0,-1}h^*_{-2,0} - 2h_{1,0}h^*_{-1,1} \end{aligned} \tag{2.1.19}$$

Each rf photocurrent outputs an rms power into the load resistance, R_{load}, that is proportional to the square of the dc current.

$$P_{f_1} = \frac{1}{2}R_{load}i^2_{dc}X_0^{-2}\beta_1^2\left|X_1\right|^2 \tag{2.1.20}$$

$$P_{2f_1} = \frac{1}{32}R_{load}i^2_{dc}X_0^{-2}\beta_1^4\left|X_2\right|^2 \tag{2.1.21}$$

$$P_{2f_1-f_2} = \frac{1}{128}R_{load}i^2_{dc}X_0^{-2}\beta_1^4\beta_2^2\left|X_3\right|^2 \tag{2.1.22}$$

In this section, I have derived closed form expressions for the photocurrents at different frequencies at the output of a filtered FM link. A general result has been given in (2.1.9) which includes residual intensity modulation, and can be solved to arbitrary precision by taking a large number of terms in the infinite sum. A small signal approximation, (2.1.10), gives the output current at any frequency component of interest. Expressions for the photocurrent at the fundamental, second harmonic and third order intermodulation distortion have been derived, which will be useful in expressing figures of merit for distortion and dynamic range.

2.2 Signal to noise ratio

In this section, I derive the signal to noise ratio (SNR) for the small signal approximation of an arbitrary link. A passive link with no amplification will be considered, so the primary noises seen at the detector are shot, thermal, phase and RIN. The shot noise spectral density is proportional to the dc from the photodetector and q, the elementary charge. The thermal noise spectral density is equal to the product Boltzmann's constant, k_B, and the temperature, T_K.

$$S_{sn} = 2qi_{dc}R_{load} \tag{2.2.1}$$

$$S_{tn} = k_B T_K \tag{2.2.2}$$

Assuming a Lorentzian model for the laser's spectral line, the phase noise on the optical carrier is white noise with spectral density proportional to the laser's 3-dB linewidth, $\triangle\nu$ [38]. The phase fluctuations are converted to intensity fluctuations by the filter in the same manner as it converts the modulation. The average phase fluctuations in a small bandwidth near some frequency, f, are

$$\left\langle \varphi\left(t\right)^2 \right\rangle \approx \frac{\triangle\nu}{\pi}\frac{\triangle f}{f^2}$$

Near the first modulation frequency, f_1, the power spectral density of the phase noise is

$$S_{pn} \approx R_{load}\Re^2 P_{opt}^2 \frac{\triangle\nu}{\pi f_1^2}\left|X_1\right|^2 = R_{load}i_{dc}^2 X_0^{-2}\frac{\triangle\nu}{\pi f_1^2}\left|X_1\right|^2 \tag{2.2.3}$$

The modulation is assumed to be below the relaxation frequency of the laser, so the RIN is modeled as white noise. The power spectral density of the noise at the output, near the modulation frequency is

$$S_{in} \approx \frac{1}{4}R_{load}i_{dc}^2 X_0^{-2}\frac{\left\langle n\left(t\right)^2\right\rangle}{B}\left|Y_1\right|^2 \tag{2.2.4}$$

where B is the bandwidth in Hz. The total noise power is

$$P_{noise} \approx (S_{sn} + S_{tn} + S_{pn} + S_{in})\, B \tag{2.2.5}$$

The signal to noise ratio (SNR) is P_{f_1}/P_{noise}. If the SNR is phase noise-limited, which is the case for sufficient optical powers, moderate RIN, and efficient conversion of phase fluctuations into intensity fluctuations, the SNR is given by

$$SNR = \frac{1}{2}\delta_f^2 \pi / \triangle\nu B \tag{2.2.6}$$

For FM discriminators that have constant conversion efficiency over a large enough bandwidth, the upper bound on the SNR for an FM-DD link is determined by the modulation depth and linewidth of the FM laser.

2.3 Distortion

The signal distortion caused by the FM-DD link can be described by the output power at frequencies that are harmonics and mixing terms of the modulation frequencies. For now, I assume there is no residual IM. If each of the two modulation tones has equal modulation depth, $\delta_f = \delta_{f_1} = \delta_{f_2}$, the IMD's power, (2.1.22), is equal to the signal power, (2.1.20), for modulation depth $\delta_f^2 = 8 f_1 f_2 \left|X_1\right| / \left|X_3\right|$. The corresponding third-order output intercept point (OIP3) is

$$OIP3 = 4 R_{load} i_{dc}^2 X_0^{-2} f_1^{-1} f_2 \left|X_1\right|^3 / \left|X_3\right| \tag{2.3.1}$$

The second harmonic's power, (2.1.21), is equal to the signal power, (2.1.20), for modulation depth $\delta_f^2 = 16 f_1^2 \left|X_1\right|^2 / \left|X_2\right|^2$. The corresponding second-order output

intercept point (OIP2) is

$$OIP2 = 8R_{load}i_{dc}^2 X_0^{-2} \left|X_1\right|^4 / \left|X_2\right|^2 \tag{2.3.2}$$

For an arbitrary filter, the distortion will depend on the particular modulation frequencies chosen. One desires to maximize $|X_1|$ and minimize $|X_2|$ and $|X_3|$ to reduce the distortion. A link with zero $|X_2|$ or $|X_3|$ will have infinite OIP2 or OIP3.

2.4 Spurious free dynamic range

The spurious free dynamic range (SFDR) is defined as the SNR at the maximum usable modulation depth. This can be defined when either the second-order or third-order distortion products breach the noise floor. For a phase noise-limited link, the IM3 is equal to the noise power at modulation depth $\delta_f^2 = \left(128 f_1^2 f_2^2 \frac{\triangle\nu}{\pi} B\right)^{1/3} \left|X_1\right|^{2/3} / \left|X_3\right|^{2/3}$. For a link limited by IM3, using (2.2.6), the SFDR is

$$SFDR_3 = \left(\frac{4 f_1 f_2 \pi \left|X_1\right|}{B \triangle\nu \left|X_3\right|}\right)^{2/3} \tag{2.4.1}$$

For a phase noise-limited link, the power at the second-harmonic frequency is equal to the noise power at modulation depth $\delta_f^2 = 4 f_1 \sqrt{\frac{2\triangle\nu B}{\pi}} \left|X_1\right| / \left|X_2\right|$. For a link limited by the second-harmonic distortion, the SFDR is

$$SFDR_2 = \frac{2 f_1 \sqrt{2\pi} \left|X_1\right|}{\sqrt{\triangle\nu B} \left|X_2\right|} \tag{2.4.2}$$

These figures-of-merit are often defined with respect to 1 Hz bandwidth. They generally depend on the particular modulation frequencies chosen. Maximizing the ratios of $|X_1| / |X_2|$ and $|X_1| / |X_3|$ will improve the dynamic range of the link.

2.5 Specific FM discriminators

Because the bandwidth of optical systems is very large, the spectrum of optical filters can include many repeating periods. To specify the filter response, one starts with the frequency response of the filter normalized over one free spectral range (FSR), written in terms of angular frequency $\Omega = -\pi$ to π. One period of the filter is centered at a chosen center frequency f_0, which is not necessarily the same as the carrier frequency f_c. I define the bias-frequency offset of the filter as $f_b = f_c - f_0$, which can be adjusted by tuning the wavelength of the transmitting laser or the physical parameters of the optical filter. The amplitude of the transfer function corresponds to the electric field transmission of the filter. The maximum bounds on the amplitude are -1 and 1. Negative transmission corresponds to a phase shift at zero field transmission. The phase shifts between adjacent periods of the filter are determined by the filter type.

2.5.1 Mach-Zehnder interferometer

The simplest filter used as an FM discriminator is an MZI with 50% coupling ratios. One arm of the interferometer has a time shift with respect to the second arm. A normalized period of the filter is written as

$$h(\Omega) = \frac{1}{2} - \frac{1}{2}\exp(-j\Omega) \tag{2.5.1}$$

The filter is typically biased at quadrature, giving in our notation (see equ. 2.1.4) a transfer function of

$$h_{n,p} = \frac{1}{2} - \frac{j}{2}\exp\left[-j2\pi\left(nf_1 + pf_2\right)\tau\right] \tag{2.5.2}$$

where τ is the time delay between the two arms. (This is not written as $h(f)$ in order to avoid confusion between modulation and optical frequencies). The intensity

response is a sinusoid

$$h_{n,p}h_{n,p}^{*} = \frac{1}{2}\left\{1 - sin\left[-2\pi\left(nf_1 + pf_2\right)\tau\right]\right\} \tag{2.5.3}$$

Using the transfer function, I evaluate the link constants

$$X_0 = \frac{1}{2} \tag{2.5.4}$$

$$X_1 = \frac{1}{2}j\left(1 - je^{-j2\pi f_1\tau}\right) \tag{2.5.5}$$

$$X_2 = 0 \tag{2.5.6}$$

$$X_3 = -\frac{1}{2}j\left(1 - je^{j2\pi f_1\tau}\right)^2\left(1 - je^{j2\pi f_2\tau}\right)e^{-j4\pi f_1\tau} \tag{2.5.7}$$

As expected for an MZI at quadrature, I find that there is no second-harmonic so that OIP2 is infinite. Using the approximation $f_1\tau, f_2\tau \ll 1$, the absolute value of the other coefficients are

$$|X_1| = \sin\left(\pi f_1\tau\right) \approx \pi f_1\tau \tag{2.5.8}$$

$$|X_3| = 4\sin^2\left(\pi f_1\tau\right)\sin\left(\pi f_2\tau\right) \approx 4\pi^3 f_1^2 f_2\tau^3 \tag{2.5.9}$$

The power at the fundamental and IMD3 frequencies are

$$P_{f_1} = 2R_{load}i_{dc}^2\delta_{f_1}^2\pi^2\tau^2 \tag{2.5.10}$$

$$P_{2f_1-f_2} = \frac{1}{2}R_{load}i_{dc}^2\delta_{f_1}^4\delta_{f_2}^2\pi^6\tau^6 \tag{2.5.11}$$

The OIP3 of the quadrature biased MZI and the phase noise-limited SFDR are

$$OIP3 = 4R_{load}i_{dc}^2 \tag{2.5.12}$$

$$SFDR_3 = \left(\triangle\nu B\pi\tau^2\right)^{-2/3} \tag{2.5.13}$$

Both the useful bandwidth and the SFDR are improved by having a short time delay in the MZI. Identical results to (2.5.10) and (2.5.12) are found by [21] (with prefactors of $\times 4$ due to twice the current with balanced detection), which supports the general analysis.

2.5.2 Linear intensity

A number of groups have proposed or built optical filters that have a transfer function linear in optical intensity versus frequency and small group delay. Within one-half period, the transfer function can be represented by

$$h_{n,p} = \sqrt{A\left(f_b + nf_1 + pf_2\right)} \exp\left[-j2\pi\left(f_b + nf_1 + pf_2\right)\tau\right] \tag{2.5.14}$$

where A is a slope in units of inverse frequency and τ is a time delay. The intensity response is

$$h_{n,p}h_{n,p}^* = A\left(f_b + nf_1 + pf_2\right) \tag{2.5.15}$$

which is linear in slope A. Using the transfer function, I evaluate the link constants:

$$X_0 = \sqrt{Af_b}e^{-j2\pi f_b \tau} \tag{2.5.16}$$

$$X_1 = Af_b\left(\sqrt{1+\frac{f_1}{f_b}} - \sqrt{1-\frac{f_1}{f_b}}\right)e^{-j2\pi f_1 \tau} \tag{2.5.17}$$

$$\begin{aligned} X_2 = Af_b\Bigg(&\sqrt{1+2\frac{f_1}{f_b}} - \sqrt{1-\frac{f_1}{f_b}} \\ &-2\sqrt{1+\frac{f_1}{f_b}}\sqrt{1-\frac{f_1}{f_b}}\Bigg)e^{-j4\pi f_1 \tau} \end{aligned} \tag{2.5.18}$$

$$\begin{aligned} X_3 = Af_b\Bigg(&2\sqrt{1+\frac{f_1}{f_b}-\frac{f_2}{f_b}}\sqrt{1-\frac{f_1}{f_b}} \\ &-2\sqrt{1-\frac{f_1}{f_b}+\frac{f_2}{f_b}}\sqrt{1+\frac{f_1}{f_b}}\sqrt{1-2\frac{f_1}{f_b}+\frac{f_2}{f_b}} \\ &-\sqrt{1+2\frac{f_1}{f_b}-\frac{f_2}{f_b}}+\sqrt{1+2\frac{f_1}{f_b}}\sqrt{1+\frac{f_2}{f_b}} \\ &-\sqrt{1-2\frac{f_1}{f_b}}\sqrt{1-\frac{f_2}{f_b}}\Bigg)e^{-j2\pi\tau(2f_1-f_2)} \end{aligned} \tag{2.5.19}$$

$$\tag{2.5.20}$$

Generally, X_2 and X_3 are non-zero for this discriminator, even if the square roots are expanded. This means that an FM discriminator that is linear in optical intensity will still produce second-order and third-order distortion. Mixing in the photodetector produces cross terms that are not eliminated. An FM discriminator that is linear is optical intensity will not produce a distortion-less link.

2.5.3 Linear electric field

The ideal filter for an FM-DD link is an optical filter that is linear in electric field. I find that this filter has second order-distortion that is produced by the square-law detection, but no other higher-order distortion. Within one period, the field transmission ramps linearly with frequency, and the filter has linear phase. The

transfer function is

$$h_{n,p} = A\left(f_b + nf_1 + pf_2\right)\exp\left[-j2\pi\left(f_b + nf_1 + pf_2\right)\tau\right] \tag{2.5.21}$$

where A is a slope in units of inverse frequency and τ is a time delay. In the intensity domain, the filter looks quadratic.

$$h_{n,p}h_{n,p}^{*} = A^2\left(f_b + nf_1 + pf_2\right)^2 \tag{2.5.22}$$

The link constants are

$$X_0 = A^2 f_b^2 \equiv T \tag{2.5.23}$$

$$X_1 = 2A^2 f_1 f_b e^{-j2\pi f_1\tau} = 2Af_1 T^{1/2} e^{-j2\pi f_1\tau} \tag{2.5.24}$$

$$X_2 = 2A^2 f_1^2 e^{-j4\pi f_1\tau} \tag{2.5.25}$$

$$X_3 = 0 \tag{2.5.26}$$

I define the constant T to describe the dc bias of the filter, which is the fraction of optical power transmitted by the filter at the optical carrier frequency. I find the photocurrents at the output of the photodetector.

$$i_{dc} = \Re P_{opt} T \tag{2.5.27}$$

$$i_{f_1} = 2i_{dc}T^{-1/2}\delta_{f_1} A\cos\left[2\pi f_1\left(t-\tau\right)\right] \tag{2.5.28}$$

$$i_{2f_1} = \frac{1}{2} i_{dc} T^{-1}\delta_{f_1}^2 A^2\cos\left[4\pi f_1\left(t-\tau\right)\right] \tag{2.5.29}$$

The magnitude of the fundamental current is linearly proportional to the slope of the filter and linearly proportional to the frequency modulation depth δ_f . This filtered link produces distortion at the second-harmonic of each modulation tone. The distortion is caused by the first-order sidebands beating with each other. The rf

power at the fundamental and second-harmonic frequencies are

$$P_{f_1} = 2R_{load} i_{dc}^2 T^{-1} \delta_{f_1}^2 A^2 \tag{2.5.30}$$

$$P_{2f_1} = \frac{1}{8} R_{load} i_{dc}^2 T^{-2} \delta_{f_1}^4 A^4 \tag{2.5.31}$$

In the small modulation depth approximation, this ideal FM-DD link has no other higher-order distortion. Using a symbolic algebra solver, I verified that the current is zero for all intermodulation and harmonic frequencies up to sixth order. At a given harmonic, sum or difference frequency, if all the sidebands in the sum in (2.1.9) corresponding to that frequency fall within a region of the filter that closely approximates the desired linear ramp function, the output current is zero.

The second-harmonic can be suppressed if the output of the optical system is detected using balanced detection. The filter before the second photodetector is designed to have a slope complementary to the first filter. Its transfer function is

$$h''_{n,p} = A\left(f_b - nf_1 - pf_2\right) \exp\left[-j2\pi\left(f_b + nf_1 + pf_2\right)\tau\right] \tag{2.5.32}$$

The current component at the fundamental frequency will be 180° out of phase between the two photodetectors, but the second-harmonic will be in phase. Subtracting the second current from the first, the second-harmonic will cancel.

Additional sources of nonlinearity are the frequency modulated laser source, optical fibers and photodetector. For sufficient modulation depth, the dominant FM sidebands will fall outside the bandwidth of the filter and this saturation will cause nonlinearities.

2.6 Optimization of the linear link

2.6.1 Gain, noise figure and low biasing

Low biasing the filter, meaning that f_c is very close to the zero transmission point at f_0, has been suggested to improve the noise figure (NF) of an FM link. However, there is a tradeoff between decreasing the dc, which decreases shot noise, and reducing the signal gain, so an optimal bias point must be found. The filter cannot be biased exactly at the null or the link would have zero output current, since I find in (2.5.28) that the output is proportional to the bias. This is consistent with experience with carrier suppression on IM-DD links.

The noise contribution from optical phase noise is

$$S_{pn} = 4R_{load} i_{dc}^2 T^{-1} A^2 \frac{\triangle \nu}{\pi} \tag{2.6.1}$$

To find the gain and noise figure of the link, the frequency modulation depth should be written in terms of the FM laser modulation parameters. It is proportional to the modulation efficiency η, in units of Hz/A, typically of the order of a few hundred MHz per mA. The peak input current, i_{in} produces an rms input power P_{in} when delivered to a load resistance R_{load}.

$$\delta_{f_1}^2 = (\eta i_{in})^2 = 2\eta^2 P_{in}/R_{load} \tag{2.6.2}$$

Assuming equal input and output loads, the power gain of the link is

$$G = 4 i_{dc}^2 T^{-1} \eta^2 A^2 \tag{2.6.3}$$

The noise figure of the link is given by the ratios of the input and output SNRs, assuming a thermal noise limited input. I assume that the dominant sources of noise

are phase, shot and thermal noises at temperature T_K. The relative intensity noise is suppressed through the balanced detection.

$$NF = 1 + \frac{1}{G} + \frac{2qi_{dc}R_{load} + 4R_{load}i_{dc}^2 T^{-1} A^2 \frac{\triangle\nu}{\pi}}{Gk_B T_K} \tag{2.6.4}$$

$$= 1 + \frac{1}{G} + R_{load}\frac{Tq + 2i_{dc}A^2\frac{\triangle\nu}{\pi}}{2i_{dc}\eta^2 A^2 k_B T_K} \tag{2.6.5}$$

A useful question is whether it makes sense to low bias the filter in an attempt to improve the noise figure. The answer depends on whether the designer is limited by optical power available or by the maximum photocurrent the photodetectors can handle. In the shot noise limited regime, the noise figure is improved by low biasing the filter, as long as the optical power is increased to maintain a fixed dc photocurrent

$$NF_{sn} \approx 1 + \frac{T}{4i_{dc}^2\eta^2 A^2} + R_{load}\frac{Tq}{2i_{dc}\eta^2 A^2 k_B T_K} \tag{2.6.6}$$

For a fixed current, for which the optical power is increased to maintain, the derivative of the NF with respect to the bias is

$$\frac{\partial NF}{\partial T} = \frac{1}{4i_{dc}^2\eta^2 A^2} + R_{load}\frac{q}{2i_{dc}\eta^2 A^2 k_B T_K}$$

The noise figure is always improved by reducing the bias. However, the phase noise will begin to dominate over the shot noise when $Tq < 2i_{dc}A^2\frac{\triangle\nu}{\pi}$, and any NF improvement will be negligible. For example, with $\triangle\nu = 1\,\mathrm{MHz}$ and $A = 1/50\,\mathrm{GHz}$, choosing a bias point $\sqrt{T} < 0.5$ only makes sense if the maximum dc current is less than $160\,\mu\mathrm{A}$.

If the available optical power is fixed, $i_{dc} = \Re P_{opt} T$, then the derivative of the NF with respect to the bias is always negative. It only serves to reduce the gain of the link and the NF gets worse with the lower bias. For high optical powers, the NF is

Figure 2.6.1: Phase noise limited noise figure versus linewidth and modulation efficiency

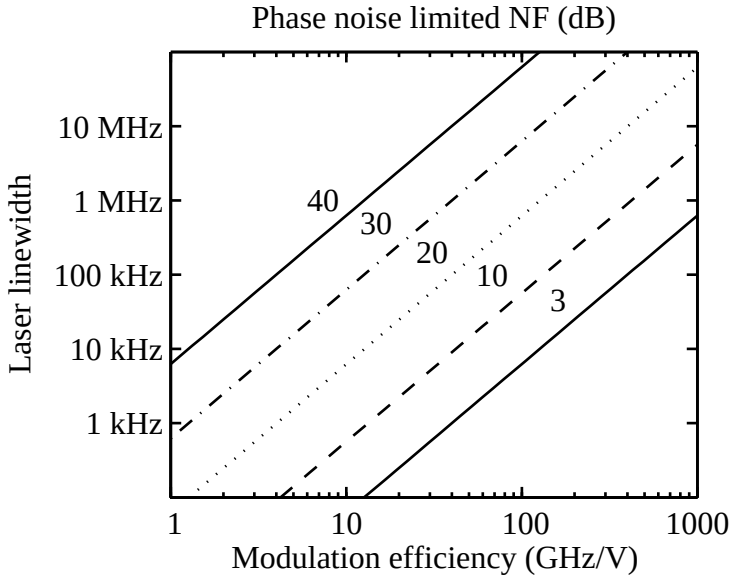

phase noise limited:

$$NF_{pn} \approx 1 + R_{load}\frac{\triangle\nu}{\eta^2 k_B T_K \pi} \tag{2.6.7}$$

This is independent of the filter bias and the slope of the filter. Because random frequency fluctuations are added to the optical carrier at the same time as it is modulated, the maximally achievable SNR is set at the laser, and cannot be improved by the rest of the system. This formula sets a fundamental relationship between the maximally achievable noise figure, the laser linewidth and the modulation efficiency. For a given noise figure and modulation efficiency, the maximum laser linewidth is

$$\triangle\nu = (NF_{pn} - 1)\,\frac{\eta^2 k_B T_K \pi}{R_{load}} \tag{2.6.8}$$

This fundamental relationship between modulation efficiency, linewidth and noise figure is plotted in 2.6.1 for a range of typical values.

2.6.2 Residual intensity modulation

Residual intensity modulation sets a lower limit on the distortion for an ideal balanced-detection FM-DD link. The effect of residual IM can be obtained from (2.1.9). It is difficult to write a general expression, but it is possible to expand some individual terms. In lowest polynomial order of the modulation depth, the currents of interest are

$$i_{dc} \approx \Re P_{opt} \left|h_{0,0}\right|^2 \tag{2.6.9}$$

$$\begin{aligned} i_{f_1} \approx & \Re P_{opt} Re\left\{\left[\beta_1\left(h_{1,0}h_{0,0}^* - h_{0,0}h_{-1,0}^*\right)\right.\right. \\ & \left.\left. + \frac{1}{2}m_1\left(h_{1,0}h_{0,0}^* + h_{0,0}h_{-1,0}^*\right)e^{j\phi}\right]\exp\left[j2\pi f_1 t\right]\right\} \end{aligned} \tag{2.6.10}$$

$$\begin{aligned} i_{2f_1} \approx & \Re P_{opt}\frac{1}{4}Re\left\{\left[\beta_1^2\left(h_{2,0}h_{0,0}^* - 2h_{1,0}h_{-1,0}^* + h_{0,0}h_{-2,0}^*\right)\right.\right. \\ & \left.\left. + m_1\beta_1\left(h_{2,0}h_{0,0}^* - h_{0,0}h_{-2,0}^*\right)e^{j\phi} + \frac{1}{2}m_1^2 h_{1,0}h_{-1,0}^* e^{j2\phi}\right]\right. \end{aligned} \tag{2.6.11}$$

$$\left.\exp\left[j4\pi f_1 t\right]\right\} \tag{2.6.12}$$

$$\begin{aligned} i_{2f_1-f_2} \approx & \Re P_{opt}\frac{1}{8}Re\left\{\left[\beta_1^2\beta_2\left(-h_{2,-1}h_{0,0}^* + h_{2,0}h_{0,1}^* + 2h_{1,-1}h_{-1,0}^*\right.\right.\right. \\ & \left.\left.\left. - 2h_{1,0}h_{-1,1}^* - h_{0,-1}h_{-2,0}^* + h_{0,0}h_{-2,1}^*\right)\right. \\ & + m_1\beta_1\beta_2 e^{j\phi}\left(h_{2,0}h_{0,1}^* - h_{2,-1}h_{0,0}^* + h_{0,-1}h_{-2,0}^* - h_{0,0}h_{-2,1}^*\right) \\ & + \frac{1}{2}m_2\beta_1^2 e^{-j\phi}\left(h_{2,0}h_{0,1}^* + h_{2,-1}h_{0,0}^* - 2h_{1,0}h_{-1,1}^*\right. \\ & \left. - 2h_{1,-1}h_{-1,0}^* + h_{0,0}h_{-2,1}^* + h_{0,-1}h_{-2,0}^*\right) \\ & + m_1^2\beta_2 e^{j2\phi}\left(-h_{1,-1}h_{-1,0}^* + h_{1,0}h_{-1,1}^*\right) \\ & + \frac{1}{2}m_1 m_2\beta_1\left(h_{2,0}h_{0,1}^* + h_{1,-1}h_{-1,0}^* - h_{1,0}h_{-1,1}^* - h_{0,-1}h_{-2,0}^*\right) \\ & \left.\exp\left[j2\pi\left(2f_1 - f_2\right)t\right]\right\} \end{aligned} \tag{2.6.13}$$

For the linear-field filter, these can be written as

$$i_{dc} \approx \Re P_{opt} T \tag{2.6.14}$$

$$i_{f_1} \approx i_{dc} Re\left\{\left[\delta_{f_1} 2AT^{-1/2} + m_1 e^{j\phi}\right] \exp\left[j2\pi f_1 (t-\tau)\right]\right\} \tag{2.6.15}$$

$$\begin{aligned} i_{2f_1} \approx i_{dc} Re\Bigg\{\Bigg[&\delta_{f_1}^2 \frac{1}{2} A^2 T^{-1} + m_1 \delta_{f_1} T^{-1/2} A e^{j\phi} \\ &+ m_1^2 \frac{1}{8}\left(1 - A^2 f_1^2 T^{-1}\right) e^{j2\phi}\Bigg] \exp\left[j4\pi f_1 (t-\tau)\right]\Bigg\} \end{aligned} \tag{2.6.16}$$

$$\begin{aligned} i_{2f_1-f_2} \approx i_{dc} Re\Bigg\{&m_1 \delta_{f_1} \delta_{f_2} \frac{1}{2} A^2 T^{-1} e^{j\phi} + m_2 \delta_{f_1}^2 \frac{1}{4} A^2 T^{-1} e^{-j\phi} \\ &+ \frac{1}{8} m_1^2 \delta_{f_2} T^{-1/2} A e^{j2\phi} + \frac{1}{4} m_1 m_2 \delta_{f_1} T^{-1/2} A\Bigg] \end{aligned} \tag{2.6.17}$$

$$\exp\left[j2\pi (2f_1 - f_2)(t-\tau)\right]\Big\} \tag{2.6.18}$$

Since the intensity modulation is residual, the frequency modulation will be much greater than the intensity modulation. Without balanced detection, the dominant second-harmonic term is quadratic in the FM, and the dominant IMD3 terms are quadratic in FM and linear in IM. I assume the phase difference between the FM and IM is $\phi = 0$. This assumption is not necessarily correct for an external phase modulator, for which the PM and IM should be in phase, with $\phi = -\pi/2$. For a single ended detector, the distortion currents are approximately

$$i_{2f_1}(Single) \approx i_{dc} T^{-1} A^2 \frac{1}{2} \delta_{f_1}^2 \cos\left[4\pi f_1 (t-\tau)\right] \tag{2.6.19}$$

$$\begin{aligned} i_{2f_1-f_2}(Single) \approx i_{dc} T^{-1} A^2 \frac{1}{4}&\left(m_1 \delta_{f_1} \delta_{f_2} 2 + m_2 \delta_{f_1}^2\right) \\ &\cos\left[2\pi (2f_1 - f_2)(t-\tau)\right] \end{aligned} \tag{2.6.20}$$

With balanced detection, the dominant second-harmonic terms are linear in the IM, and terms even in A cancel in the balanced detection. The dominant IMD3 terms are

quadratic in the IM, and terms even in A also cancel. The currents are approximately

$$i_{2f_1}\left(Balanced\right) \approx i_{dc} T^{-1/2} m_1 \delta_{f_1} A \cos\left[4\pi f_1 \left(t-\tau\right)\right] \tag{2.6.21}$$

$$i_{2f_1-f_2}\left(Balanced\right) \approx i_{dc} T^{-1/2} \frac{1}{8} A \left(2 m_1 m_2 \delta_{f_1} + m_1^2 \delta_{f_2}\right) \cos\left[2\pi\left(2f_1 - f_2\right)\left(t-\tau\right)\right] \tag{2.6.22}$$

It is useful to normalize the IM to the FM. One method of normalization is to look at the optical power the IM and FM contribute to the first-order optical sidebands in the small signal approximation. The optical power in the first order sidebands from the IM is $P_{opt} m_1^2/16$. The optical power in the first order sidebands due to the FM is $P_{opt}\delta_{f_1}^2/4f_1^2$. I define a relative residual IM, Γ, by

$$\sqrt{\frac{m_1^2/16}{\delta_{f_1}^2/4f_1^2}} = \frac{m_1}{\delta_{f_1}}\frac{f_1}{2} = \frac{\eta_m}{\eta}\frac{f}{2} \equiv \Gamma \tag{2.6.23}$$

where η is the FM modulation efficiency and η_m the IM modulation efficiency. A second quantity that should be normalized is the RF photocurrents due to the FM and IM after the discriminator. Using (2.6.15), the ratio of the amplitude of the two currents is

$$\frac{\left|i_f\left(FM\right)\right|}{\left|i_f\left(IM\right)\right|} = \frac{2A\delta_{f_1}}{m_1\sqrt{T}} = \frac{\Gamma_0}{\Gamma} \tag{2.6.24}$$

where I define a discriminator gain parameter

$$\Gamma_0\left(f\right) \equiv \frac{Af}{\sqrt{T}} \tag{2.6.25}$$

Using the above normalizations, the values for RIM limited OIP2 and OIP3 are

$$OIP2\,(Single) = 32 R_{load} i_{dc}^2 \tag{2.6.26}$$

$$OIP3(Single) = \frac{8}{3} R_{load} i_{dc}^2 \frac{\Gamma_0}{\Gamma} \tag{2.6.27}$$

$$OIP2\,(Balanced) = 2 R_{load} i_{dc}^2 \left(\frac{\Gamma_0}{\Gamma}\right)^2 \tag{2.6.28}$$

$$OIP3(Balanced) = \frac{8}{3} R_{load} i_{dc}^2 \left(\frac{\Gamma_0}{\Gamma}\right)^2 \tag{2.6.29}$$

The output intercept points are related to powers of the ratio of RF photocurrents caused by the FM and IM. For FM-DD links to exhibit superior third-order and second-order distortion performance, the FM laser must be optimized for low residual IM.

Chapter 3

Numerical link analysis

In order to achieve linear discrimination of optical FM, I desire to closely approximate the ideal linear-field optical filter. As reviewed by [39], optical filters can be designed using digital filter design techniques, by specifying the coefficients of the z-transform representation of the filter. The problem of discriminator design reduces to one of choosing the best coefficients. A physically-realized optical filter is limited in its number of stages so it will only closely approximate the desired linear frequency response.

Finite impulse response (FIR) filters, with all zeros and no poles in their z-transform representations, may work well as FM discriminators because symmetric FIRs can be designed to have exactly linear phase. In this chapter, I present two sets of FIR coefficients chosen using the maximally linear and minimax relative error criteria [40].

The performance of the resulting filters in links are analyzed using the small signal model, full signal model and a numerical simulation. I compare the linearity of optical frequency discriminators based on the MRE and maximally linear criteria and find that the both sets of filters surpass the Mach Zehnder interferometer (MZI) in performance, with the maximally linear filter the better of the two. I also present

Figure 3.1.1: Numerical model of an FM photonic link with two discriminator filters and balanced detection

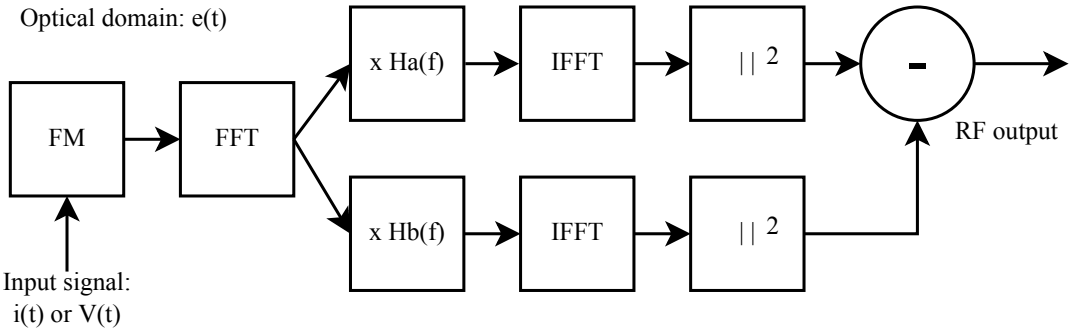

the tradeoffs between filter order, third-order nonlinearity and small signal gain.

3.1 Numerical link simulation

The signal at the output of the link is simulated by creating a time domain waveform, $e(t) \propto exp[2\pi f_c t + 2\pi\eta \int i(t)]$, performing a fast Fourier transfer (FFT), weighting the frequency domain waveform by a given filter transfer function, performing an inverse FFT and squaring the time domain waveform to obtain the photocurrent. The simulation process is illustrated in figure 3.1.1. I use a 200 GHz sampling frequency and a 10,000 point FFT to convert the time domain waveform to the frequency domain. The code for the simulation is included in Section A.1. The simulation code includes the effects of residual intensity modulation as well as imperfect common-mode rejection from the balanced photodetection.

3.2 Filter coefficients

The frequency discriminator's transfer function is similar to that of a digital differentiator filter: a ramp with constant slope. Two sets of design criteria for digital differentiators known in the literature are the minimax relative error (MRE) criteria

and the maximally linear criteria (maxlin). The MRE criteria minimize the maximum relative error over a chosen band of frequencies. The maximally linear criteria fix a number of derivatives of the transfer function at a chosen frequency, guaranteeing high accuracy around a small frequency band. If this band is comparable to the bandwidth of our modulation, overall I expect high linearity.

I obtain coefficients for MRE filters by numerically optimizing at half-band, over the range of normalized frequencies 0.45π to 0.55π (2π is the full FSR). The coefficients obtained for the MRE filters are shown in Table 3.2.1 on page 44. The maximally linear filter is also optimized at half-band, at the point $\Omega = \pi/2$. The coefficients of second, sixth, tenth and fourteenth-order, maxlin filters are shown in Table 3.2.2 on page 44 along with the corresponding coefficients for a Mach Zehnder interferometer. The filter coefficients are illustrated in Figure 3.2.1 on page 42. The transfer functions of the filters are compared with respect to the ideal one in Figure 3.2.2 on page 43. For any given order, the maximally linear filter appears to more closely approximate the linear discriminator. This example does not preclude the possibility that better MRE coefficients could be found using a different numerical optimizations. The fact that the MRE filter is a Type III linear phase FIR filter (odd-length, anti-symmetric) and the maxlin filter is a Type I linear phase FIR filter (odd-length, symmetric) also affects the comparison.

3.3 Comparision of models

To verify the analytical small signal model derived in this work, I compare the small signal model (Section A.2) with the large signal (Section A.3) and numerical models (Section A.1). The parameters used in the simulation are listed in Table 3.3.1 on page 45. The third-order performance of a link with an MZI is shown in Figure 3.3.1 on page 46. The three models are consistent up through modulation powers such that

Figure 3.2.1: Filter coefficients for tenth-order MRE and maximally linear filters

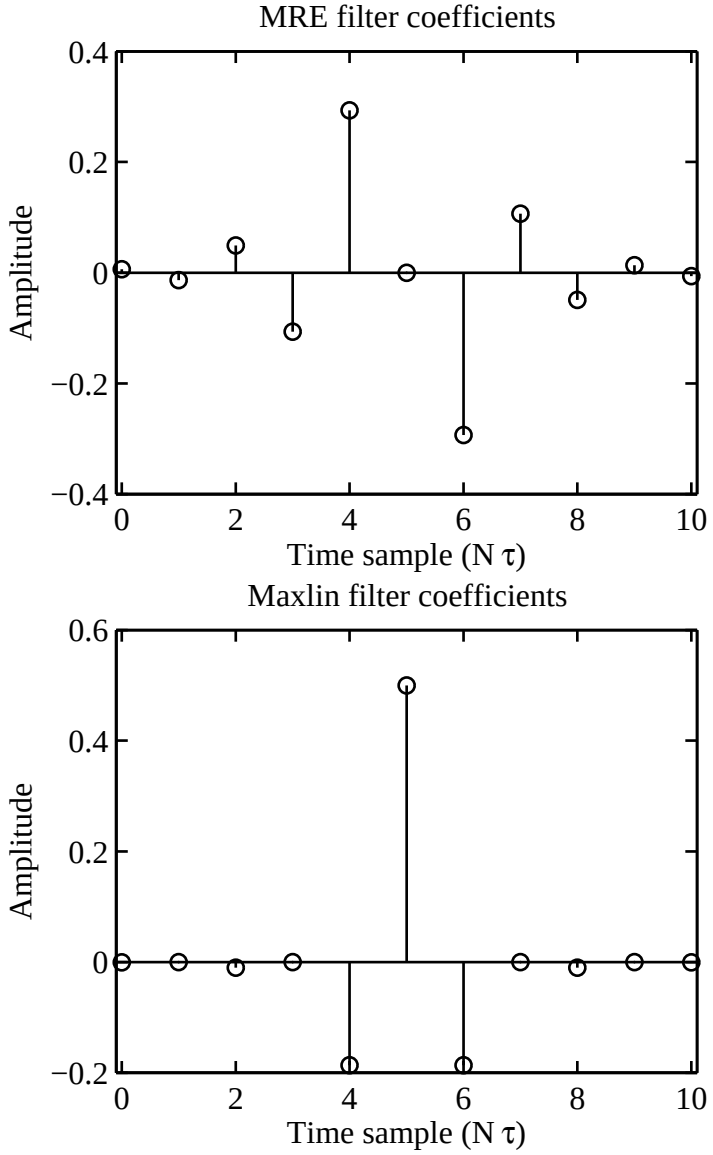

Figure 3.2.2: Transfer functions for MRE and maximally linear filters compared to ideal discriminator transfer function

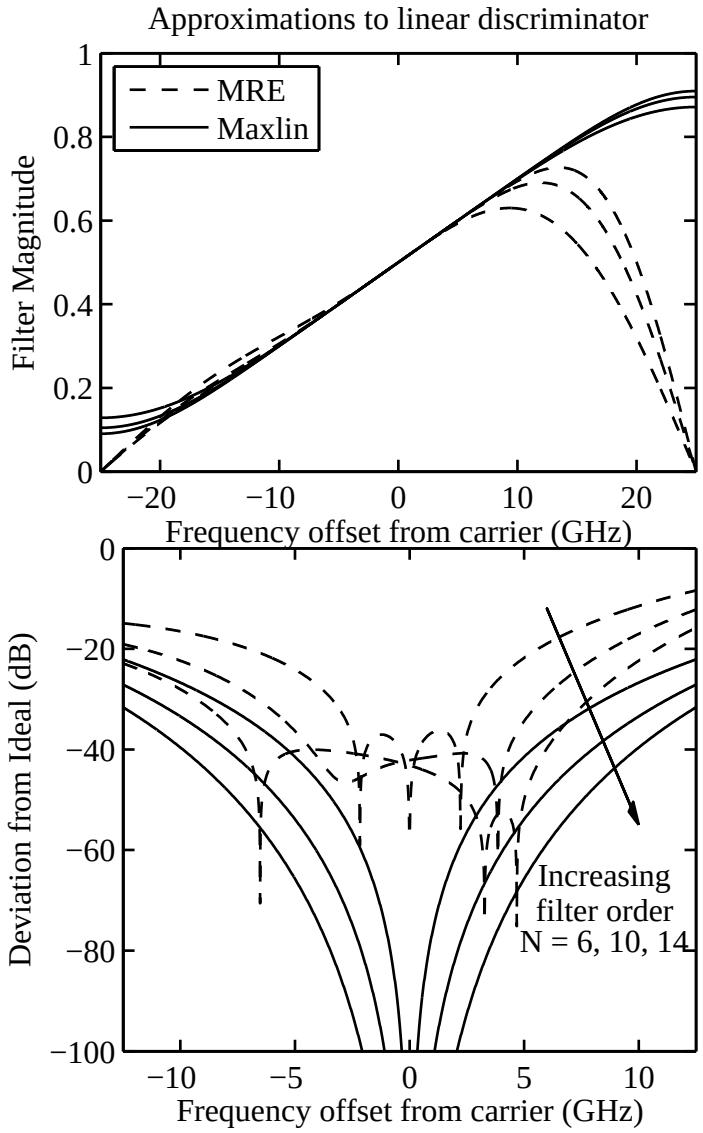

Table 3.2.1: Filter coefficients chosen using the MRE criteria for 6th, 10th and 14th order filters in z-transform representation

Order	6	10	14
a0	0.0318	0.0060306	0.0012721
a1	-0.0806	-0.01359	-0.0027526
a2	0.2818	0.0493	0.012216
a3	0	-0.1068	-0.02426
a4	-0.2818	0.2933	0.060268
a5	0.0806	0	-0.1199
a6	-0.0318	-0.2933	0.2993
a7		0.1068	0
a8		-0.0493	-0.2993
a9		0.01359	0.1199
a10		-0.0060306	-0.060268
a11			0.02426
a12			-0.012216
a13			0.0027526
a14			-0.0012721

Table 3.2.2: Filter coefficients for the MZI and 2nd, 6th, 10th and 14th order maxlin filters in z-transform representation

Order	MZI	2	6	10	14
a0	$\frac{-1}{2}$	$\frac{-1}{2\pi}$	$\frac{-1/3}{(2\pi)2^3}$	$\frac{-3/5}{(2\pi)2^7}$	$\frac{-10/7}{(2\pi)2^{11}}$
a1	$\frac{1}{2}$	$\frac{1}{2}$	0	0	0
a2		$\frac{-1}{2\pi}$	$\frac{-9}{(2\pi)2^3}$	$\frac{-25/3}{(2\pi)2^7}$	$\frac{-98/5}{(2\pi)2^{11}}$
a3			$\frac{1}{2}$	0	0
a4			$\frac{-9}{(2\pi)2^3}$	$\frac{-150}{(2\pi)2^7}$	$\frac{-490/3}{(2\pi)2^{11}}$
a5			0	$\frac{1}{2}$	0
a6			$\frac{-1/3}{(2\pi)2^3}$	$\frac{-150}{(2\pi)2^7}$	$\frac{-2450}{(2\pi)2^{11}}$
a7				0	$\frac{1}{2}$
a8				$\frac{-25/3}{(2\pi)2^7}$	$\frac{-2450}{(2\pi)2^{11}}$
a9				0	0
a10				$\frac{-3/5}{(2\pi)2^7}$	$\frac{-490/3}{(2\pi)2^{11}}$
a11					0
a12					$\frac{-98/5}{(2\pi)2^{11}}$
a13					0
a14					$\frac{-10/7}{(2\pi)2^{11}}$

Table 3.3.1: Simulation parameters

Parameter	Value
f_1 (GHz)	1.9
f_2 (GHz)	2.0
Impedances (ohms)	50
Modulation efficiency (GHz/V)	200
Laser linewidth (MHz)	0.5
Filter free spectral range (GHz)	100
Optical power before filters (mW)	100
Optical power incident upon each detector (mW)	12.5
Photodetector responsivity (A/W)	0.8
Total DC photocurrent (mA)	20
Third-order IMD (GHz)	1.8
Second harmonic (GHz)	3.8

the fundamental output starts to saturate.

The third-order performance of a link with a tenth-order maxlin filter is shown in Figure 3.3.2 on page 46. The three models are consistent for small-modulation depths. For small-modulation depths, the maxlin filter has IMD3 several orders of magnitude less than the MZI. However, the small-signal model does not capture the fast increase in power measured at frequency $2f_1 - f_2$ at larger modulation depths. The effect is due to increasing amounts of optical power in the sidebands that fall outside of the portion of the filter that is optimized for linearity. The bandwidth occupied by the modulation is approximately given by Carson's rule. The MZI link does not produce second-order distortion. With balanced detection, the maxlin link has very little second-order distortion. Assuming a common-mode rejection ratio of 30 dB, the distortion is plotted in Figure 3.3.3 on page 47.

3.4 Comparison of filters

Using the numerical and small signal models, I compare the distortion performance for the two different filter optimizations. The fundamental and third-order distortion

Figure 3.3.1: Third-order performance of an FM-DD link with an MZI discriminator

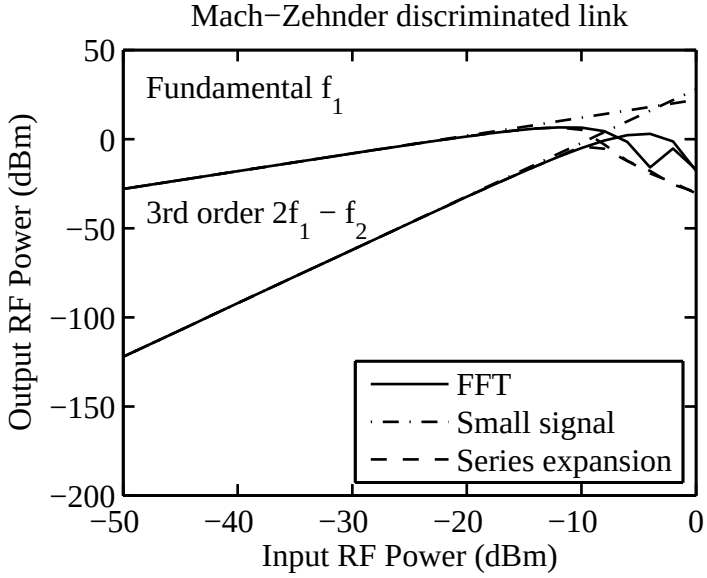

Figure 3.3.2: Third-order performance of an FM-DD link with a maxlin discriminator

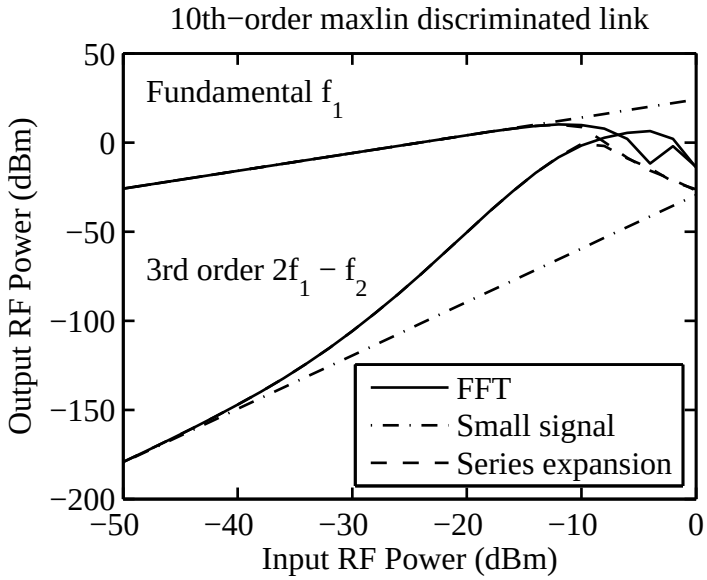

Figure 3.3.3: Second-order performance of an FM-DD link with a maxlin discriminator

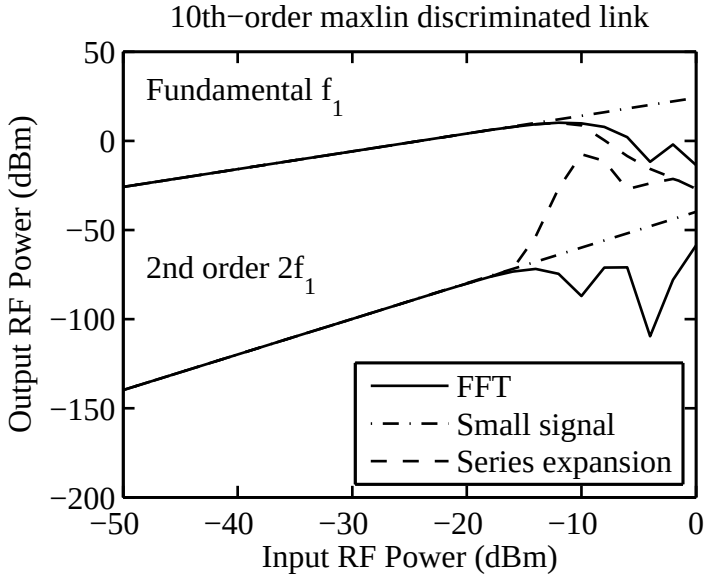

powers are plotted in Figure 3.4.1 on page 48 and the second-order distortion in Figure 3.4.2 on page 48. The noise floor is calculated using the small signal model, assuming a 500 kHz laser linewidth. In general, the higher-order filters have less distortion than the lower-order filters.

The distortion of links using either type of filter increases much faster than 30 dB / decade for large modulation power. This can be explained by observing that in frequency modulation, the frequency deviation of the carrier increases with modulation depth, so more optical power is spread into higher order sidebands. For high modulation depths, most of the optical power lies outside of the range of frequencies for which the filter is optimized, creating more distortion than for low modulation depths.

The FSR of the filter is a design parameter, which is determined by the delay elements in the implementation. A smaller FSR gives a larger slope, meaning better conversion efficiency from FM to AM and more link gain. It can also affect the linearity. Figure 3.4.3 on page 49 shows OIP3 from the small signal model versus the FSR of the filter and Figure 3.4.4 on page 50 shows the tradeoff between OIP3 and

Figure 3.4.1: Third-order distortion versus filter length and type

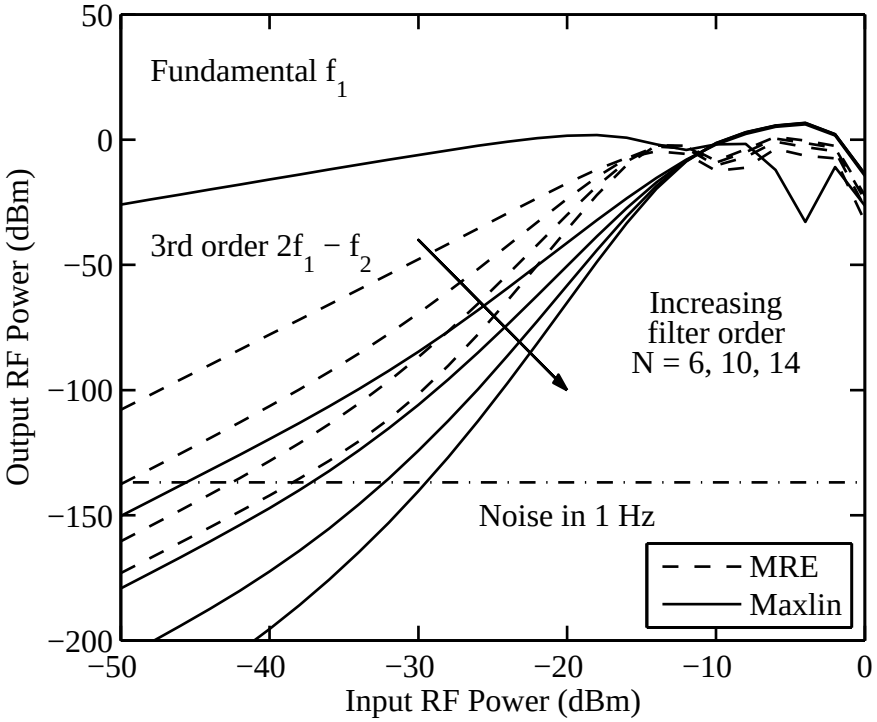

Figure 3.4.2: Second-order distortion versus filter length and type

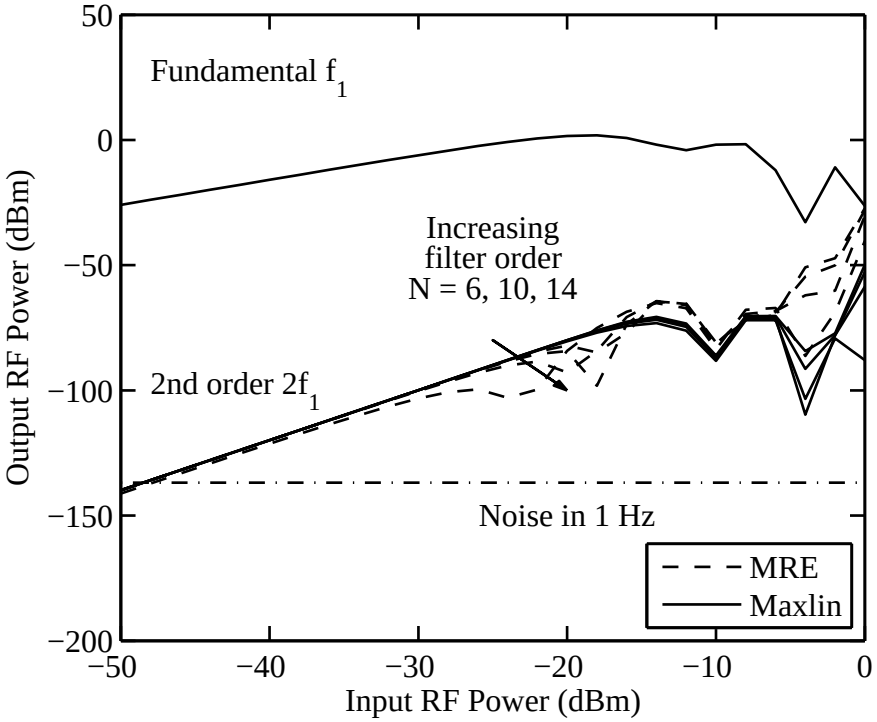

Figure 3.4.3: Third-order distortion versus filter free spectral range

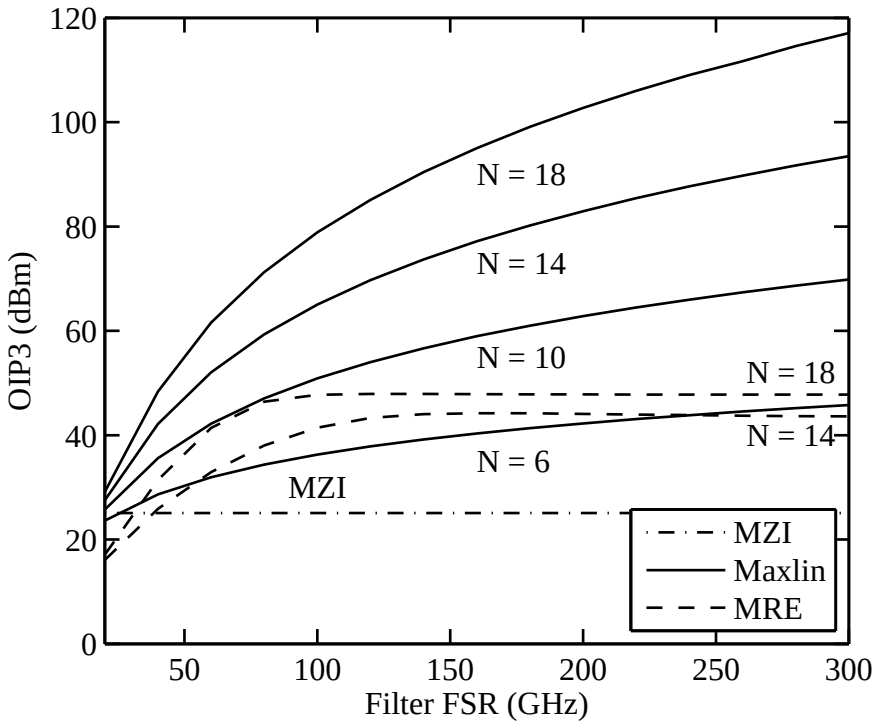

gain for the maxlin filters. By increasing the FSR, the third-order distortion decreases much faster than the gain, thus the OIP3 improves. Taking advantage of this effect is limited because the noise figure degradation will reduce the SFDR, and residual IM affects the linearity more for less efficient discrimination. Figure 3.4.5 on page 50 shows the SFDR versus FSR calculated using the numerical model to find where the noise floor and IMD3 intercept. Saturation of the achievable SFDR is clearly evident. The choice of filter FSR must carefully balance these design issues.

For maximally linear filters with larger FSRs, the third-order distortion decreases faster than the gain decreases, so OIP3 monotonically increases. Higher order filters have increasingly better distortion characteristics: by increasing the filter order by four, the OIP3 increases by 20 dB or more. The maximally linear filters are much better than the MRE filters for a given filter order. The 14th-order MRE has higher OIP3 than the sixth-order maximally linear filter, but lower OIP3 than the tenth-

Figure 3.4.4: Tradeoff between small signal gain and OIP3

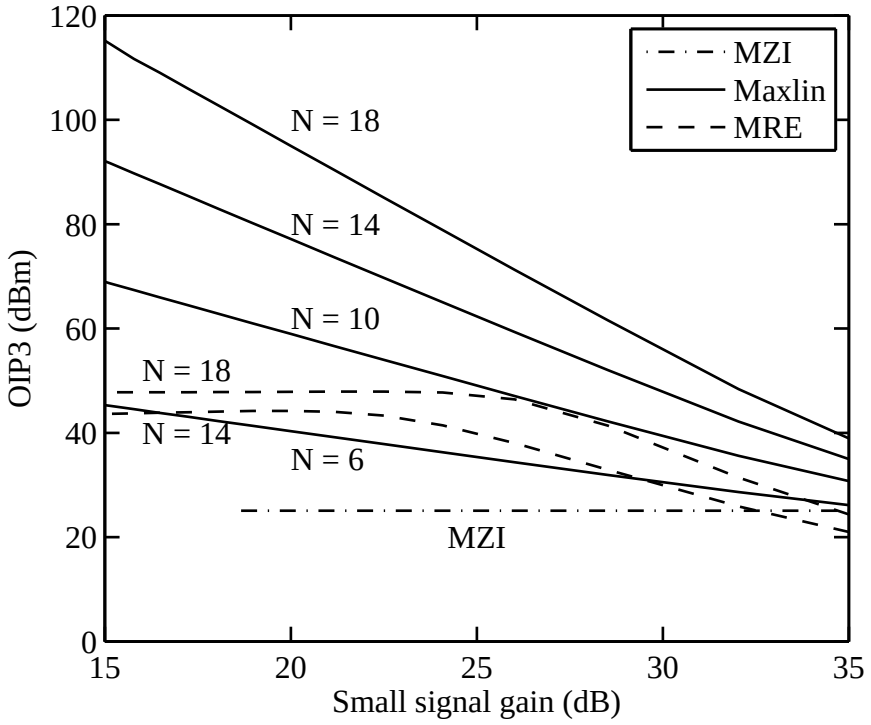

Figure 3.4.5: Third-order spurious-free dynamic-range versus filter free spectral range

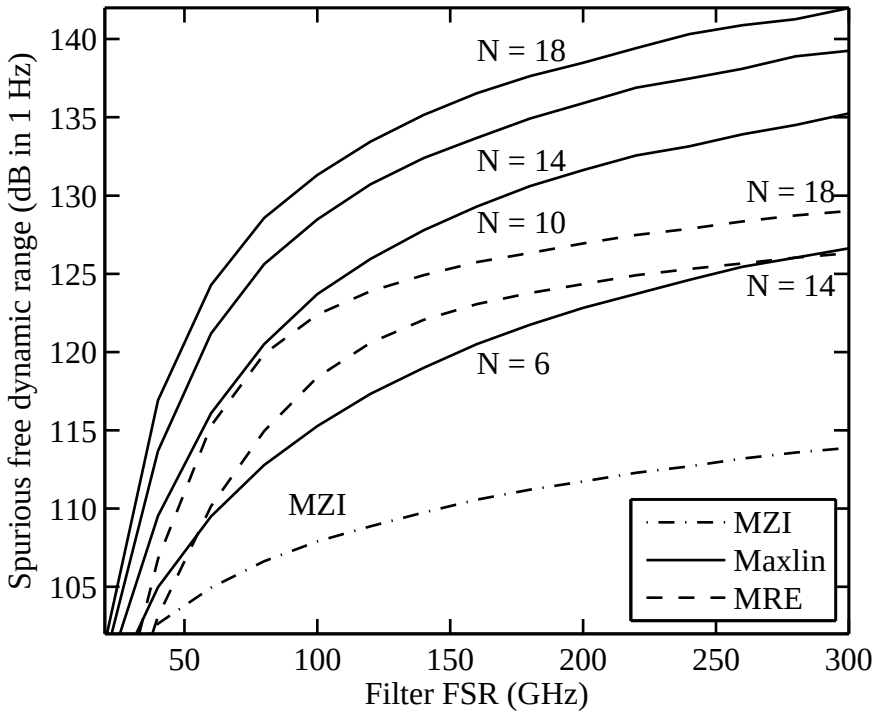

order maximally linear filter. Our results suggest that a microwave-photonic link using a 250 GHz FSR, tenth-order maximally linear filter as a frequency discriminator provides 20 dB improvement in SFDR over a MZI discriminator.

Chapter 4

Filter implementation

4.1 Planar lightwave circuit filters

An FM discriminator approximating the ideal linear field response can be constructed using planar lightwave circuites (PLC). The transform function of an FIR filter can be realized in PLC with just MZIs and directional couplers. One implementation of a multi-stage optical FIR filter in PLC is the lattice filter. The lattice filter architecture has a low-loss passband and requires only N+1 couplers for an Nth order filter, which are advantages over other optical filter architectures. The lattice filter architecture is shown in Figure 4.1.1 on page 53, indicating for each stage the coupling coefficients, designated by κ, and the phase shifts, designated by φ. Each stage has a unit delay, z^{-1}. The dashed lines indicate additional filter stages ommitted from the figure. A recursion relation exists that transforms between given filter coefficients and the corresponding coupling ratios and phase shifts [39]. The recursion relation for the lattice filter design gives 1024 solutions for a tenth-order filter. One particular solution is listed in Table 4.1.1 on page 53.

Up to tenth-order FIR lattice filters have been implemented in PLC for various applications. A research group at NTT laboratories has extensively explored tunable

Figure 4.1.1: FIR lattice filter architecture

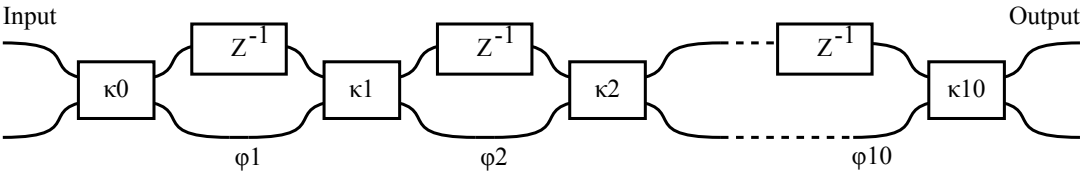

Table 4.1.1: Filter phase and coupler parameters for a tenth-order maxlin discriminator

Phase shift	Value	Coupling ratio	Value	Tunable coupler phase
φ_1	0	κ_0	0.674271	0.607391
φ_2	$-\pi$	κ_1	0.635460	0.648224
φ_3	0	κ_2	0.837472	0.414954
φ_4	$-\pi$	κ_3	0.514751	0.770645
φ_5	0	κ_4	0.918512	0.289487
φ_6	0	κ_5	0.538578	0.746782
φ_7	$-\pi$	κ_6	0.918384	0.289721
φ_8	0	κ_7	0.515217	0.770179
φ_9	$-\pi$	κ_8	0.837319	0.415161
φ_{10}	$-\pi$	κ_9	0.635828	0.647842
		κ_{10}	0.325694	0.963443

optical FIR lattice filters. Tunable coupling ratios are implemented by using symmetric Mach-Zehnder interferometers with thermal-optic phase shifters. A diagram of a tunable FIR filter is shown in Figure 4.1.2 on page 55. The intended application is dispersion compensation, but because the filters are tunable, they can be used for any filter transfer function desired, including FM discriminators.

The group has fabricated eight-order filters in silica with chromium heaters, with 50 GHz FSR [41] and 200 GHz FSR [42], and arrays of fifth-order filters with 50 GHz FSR [43, 44, 45]. They claim control of the individual phase shifters to accuracy better than 0.01π radians. For the fifth-order filters, to reduce the required bias power on the heaters, they use a phase-trimming technique that involves introducing heating induced stress. They have also proposed a 100 GHz FSR filter in a reflection configuration to double its effective length [46].

A collaboration between Siemens, University of Kiel and IBM Research Zurich has implemented the same architecture on a more compact silicon oxynitride platform [47]. The applications include both EDFA gain equalization and dispersion compensation. They have demonstrated sixth, seventh and tenth-order filters with 100 GHz FSR. The collaboration has explored a number of adaptive feedback approaches for setting the filter's phase shifters [48].

- Optical spectrum analysis [49]: They have used an optical spectrum analyzer to compare the amplified spontaneous emission spectrum to a desired intensity profile. A computer running the Levenberg-Marquart optimization algorithm (a modified Gauss-Newton algorithm) varies the power to the phase shifters until the desired profile is obtained.

- Electrical spectrum monitoring [50, 51, 52]: ESM is another feedback approach, where power at certain frequencies are used as a feedback mechanism. Pilot tones or knowledge about the signaling over the link determines the optimal choice of electrical filters.

Figure 4.1.2: Tunable PLC FIR lattice filter architecture

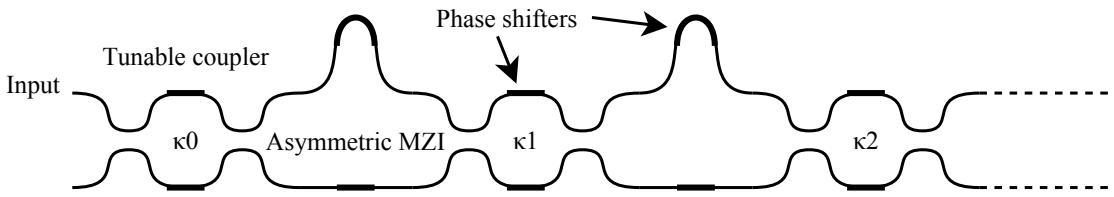

- Eye opening [53, 54, 55]: An adaptive feedback approach for digital signals looks at an eye diagram and uses a Levenberg-Marquart optimization to maximize the eye opening.

- LMSE / minimize ISI [56, 57, 58, 50, 52]: Another method for digital signals uses minimization between the decision and signal as a feedback signal. These methods are not suitable for analog links.

For simplicity and cost, setting the filters coefficients without using a feedback system is desired. The IBM collaboration has developed a calibration procedure to produce a table look-up for tunable coupler and phase shifter responses versus applied tuning power [49]. The technique uses the OSA approach to iteratively tune all couplers to zero cross coupling. There is a procedure to individually characterize each tunable coupler and asymmetric MZI by measuring the output power versus tuning. The filter then can be set to a pre-calculated inverse system. An alternative calibration approach is given by the NTT group in [59] that does not require a feedback loop. The approach uses incoherent light to characterize each tunable coupler, and coherent light to characterize the asymmetric Mach Zehnders.

4.2 Monte Carlo simulation

I perform a Monte-Carlo simulation to study the effect of imperfect tuning on the resulting link distortions caused by the filter. For a given maximum phase deviation, a

random phase, uniformly distributed between plus and minus the maximum deviation, is added to the path length of each symmetric and assymetric MZI. After each phase shift is varied, the new filter coefficients are calculated, and the resulting OIP3 and OIP2 are calculated. The simulation is performed for 100 trials. Then, the simulation is repeated, but the symmetric and assymetric MZI phase shifts are separated out to determine if the system is more sensitive to one or the other.

Figure 4.2.1 on page 57 and Figure 4.2.2 on page 58 show that OIP3 and OIP2 degrade significantly if the phases are not controlled to within 0.01 radians of their designed values. OIP2 is more sensitive to phase errors than OIP3 because the phase difference between the two photodetectors determines the cancellation of the second harmonics. The approach to setting the filter parameters, as discussed in Section 4.1, needs to be able to meet this required precision.

Figure 4.2.1: Monte Carlo simulation on third-order distortion

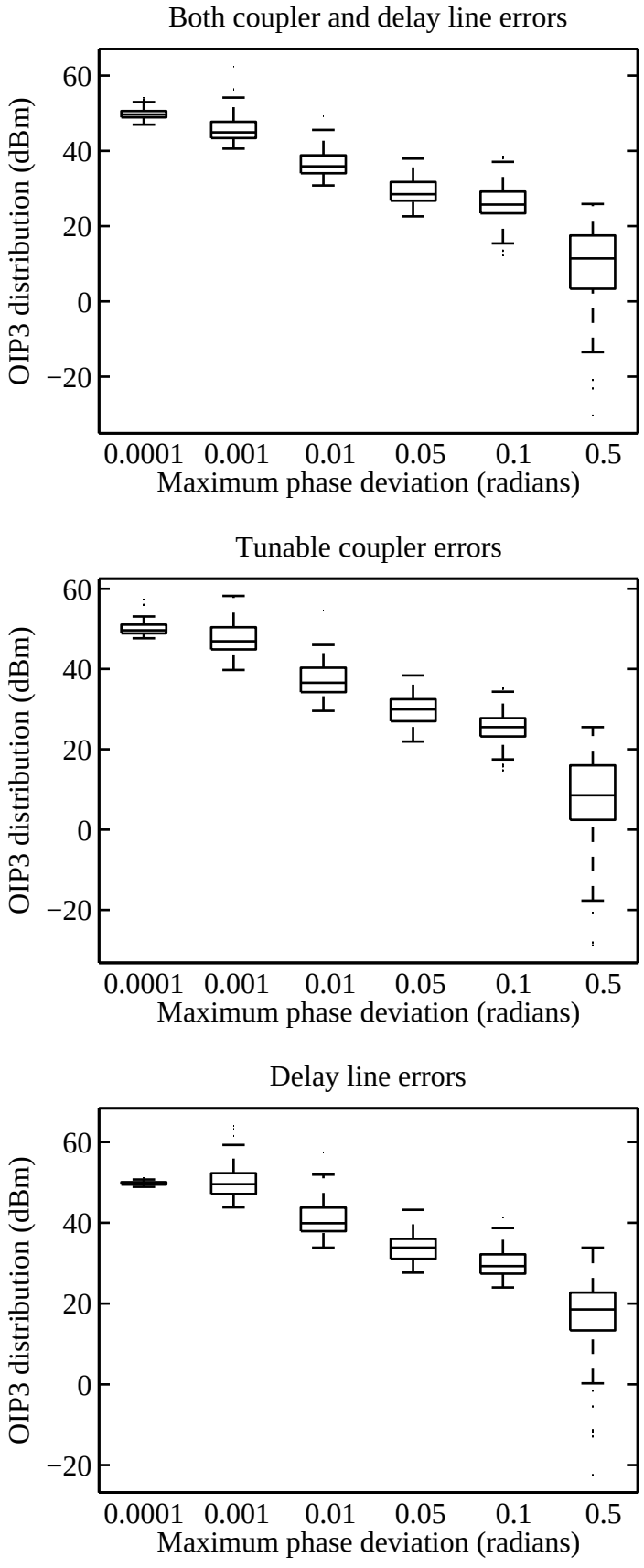

Figure 4.2.2: Monte Carlo simulation on second-order distortion

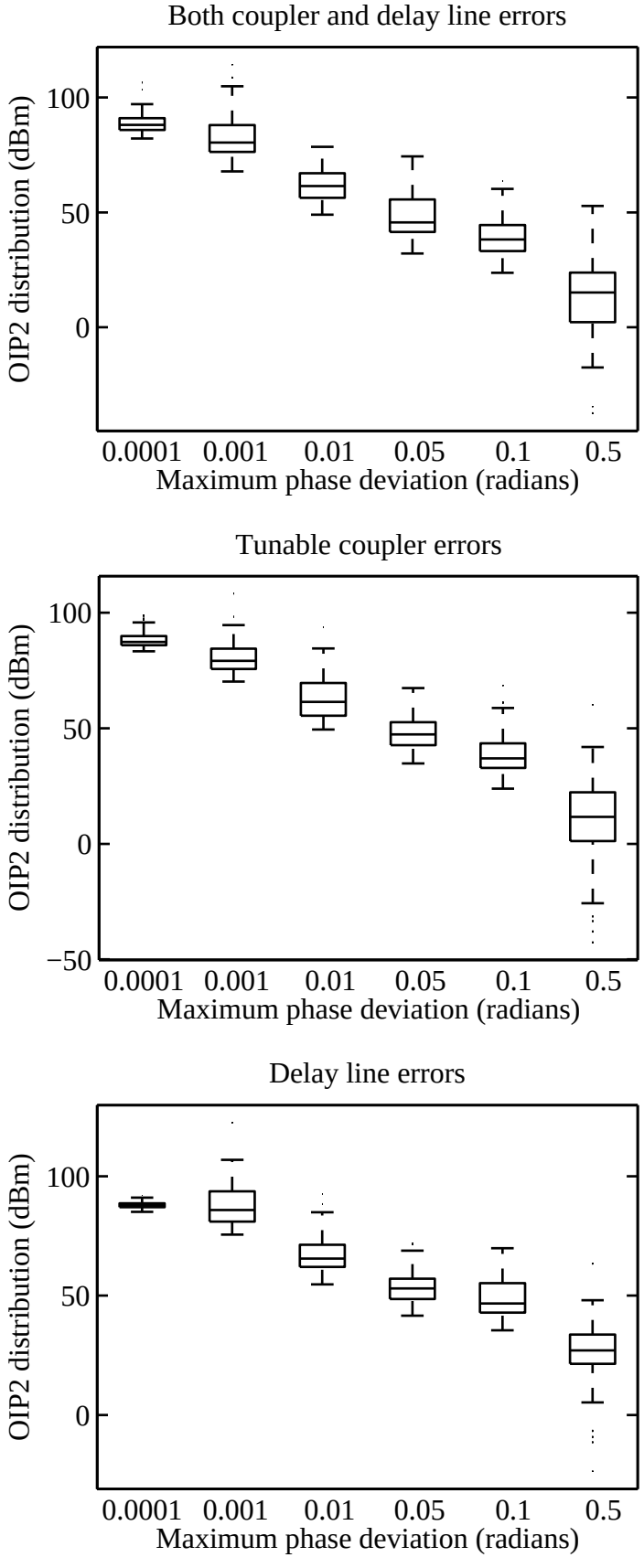

Chapter 5

Conclusions

In this report, I have presented frequency-modulated microwave photonic links with direct detection as an approach to achieving links with low noise-figure and high linearity. In Chapter 1, I have comprehensively reviewed previous work on FM discriminators, including early work with Mach Zehnder interferometers, and later attempts to linearize the links using "linear" FM to IM discriminators. I pointed out that this approach is flawed since it ignores coherence and combines an instantaneous frequency view of the modulation with a Fourier frequency spectrum view of the filter. As an alternative, I proposed balanced FM discriminator filters that are linear in field transmission versus frequency to obtain highly linear links.

In Chapter 2, I have derived large-signal and small-signal analytical expressions for the response of a filtered FM link. Using the small-signal model, I derived figures of merit for the signal to noise ratio, third-order intercept point, second-order intercept point, and spurious free dynamic range for a link with any arbitrary filter. The theory has been shown to be consistent with previous work on MZIs. A filter with a linear FM to IM ramp has been shown to generate large amounts of distortion, while a filter with a linear FM to AM ramp theoretically would not produce any third-order or higher-order distortion.

For a link with linear FM to AM conversion, expressions for the gain and noise figure have been derived. Low biasing the filter is shown to improve the noise figure only if the photodetector is limited to very small amounts of optical power. Simplified theory on the effect of residual IM has been developed, showing that with balanced detection, OIP3 and OIP2 quadratically depend on the ratio of RF photocurrent due to FM to the RF photocurrent due to IM.

In Chapter 3, I have presented a numerical model for simulating the distortion of a filtered FM link. The numerical model was shown to be consistent with both the small-signal and large-signal models derived in this report. The numerical model was used to compare two FIR filter approximations to the linear FM to AM filter. Of the minimax relative error criteria and the maximally linear criteria for choosing the filter coefficients, the maximally linear criteria has been shown to produce lower distortion for any filter order, and to improve upon on the MZI in OIP3 and SFDR by several orders of magnitude.

Finally, in Chapter 4, I reviewed implementations of optical FIR filters using the lattice filter architecture in planar lightwave circuits. Up to tenth-order tunable arbitrary filters have been constructed on silica and silcon oxynitride platforms. I have reviewed approaches to setting the filters' phase parameters presented in the literature. I have designed an implementation of a tenth-order maxlin FIR filter using an optical lattice filter. I simulated its sensitivity to the phase variations on its component switches and delay lines using a Monte Carlo simulation and found that the phases need to be controlled to better than 0.01 radians. This analysis provides guideance for implementing a low-distortion microwave-photonic link using frequency modulation and discriminator demodulation with a tunable FIR filter. Further research will implement the filter using a silica PLC device and measure its distortion performance in an experimental link.

Appendix A

Simulation code

A.1 Numerical simulation of an FM link

The numerical model for an FM link is based on the model in Figure 3.1.1 on page 40. It includes the effects of residual intensity modulation and includes the effect of the common-mode rejection ratio.

```
function output = model_fft(param, HaF, HbF, K, fcMHz, PindBm, CMRR)
%MODEL_FFT   Numerical model for a frequency modulated link
%   Input param = [fsMHz, N, etaMHz, G, PmW, R, Rohm];
%   Input Ha, Hb are the filter transfer functions, over the range of
%        frequency offsets    f  = (-N/2:N/2-1)*fsMHz/N;
%   Input K is the optical power split [Pa/P Pb/P] between the two filters
%   Input fcMHz are the modulation frequencies in MHz [f1, f2, ...]
%   Input PindBm are the modulation powers in dBm [P1, P2, ...]
%   Input CMRR is the common mode rejection ratio for balanced detection
%        in positive decibels. Matlab accepts 'Inf' for perfect CMRR.
%   Output is power [P1, P2, ...] in dBm at frequencies
%        [f1, f2, .... fn, 2*f1, 2*f2, ... 2*fn, 2*f1-f2, 2*f2-f1]

%% Modulation %%
```

```
fsMHz    = param(1); % FFT sampling frequency
N        = param(2); % FFT number of points
etaMHz   = param(3); % Frequency modulation efficiency in MHz/mA
G        = param(4); % RIM normalization parameter
PmW      = param(5); % Optical power before the filters
R        = param(6); % Responsivity of photodetectors
Rohm     = param(7); % Input and output load impedance

% Monitor the output for second and third order distortions
monMHz = [fcMHz*2, abs(fcMHz(1)*2-fcMHz(2)),abs(fcMHz(2)*2-fcMHz(1))];

% Calculations for modulation
PinW  = 10.^((PindBm-30)/10);    % Input RMS power at each tone in Watts
IA    = sqrt(2*PinW/Rohm);       % Input peak current in Amps
ImA   = IA*1000;                 % Peak amplitudes for each tone in mA
df    = etaMHz*ImA;              % Frequency modulation depths
b     = df./fcMHz;               % Phase modulation depths
m     = G*b*2;                   % Intensity modulation depths

% Generate the time domain signal
IinT = 0; XinT = 0; YinT = 0; % Current, FM, and IM
for x = 1:length(fcMHz)
    IinT = IinT + ImA(x)/1000*sin(2*pi*fcMHz(x)*(0:N-1)/fsMHz);
    XinT = XinT + b(x)*cos(2*pi*fcMHz(x)*(0:N-1)/fsMHz);
    YinT = YinT + m(x)*sin(2*pi*fcMHz(x)*(0:N-1)/fsMHz);
end

% Generate the modulated optical signal centered at fc
EmodT = sqrt(2*PmW/1000)*sqrt(1+YinT).*exp(j*XinT);

%% Filtering %%

EmodF  = fftshift(fft(EmodT,N))/N; % Convert to the frequency domain
```

```
EoutaF = EmodF.*HaF*sqrt(K(1));      % Split and Filter
EoutbF = EmodF.*HbF*sqrt(K(2));      % Split and Filter
EoutaT = ifft(ifftshift(EoutaF),N)*N;  % Convert to time domain
EoutbT = ifft(ifftshift(EoutbF),N)*N;  % Convert to time domain

%% Detection %%

% Convert back to electrical domain
IoutaT = R*EoutaT.*conj(EoutaT)/2;
IoutbT = R*EoutbT.*conj(EoutbT)/2;
IoutT  = IoutaT - IoutbT + (IoutaT + IoutbT)*10^(-CMRR./10);

% Convert the currents to the frequency domain
IinF   = fftshift(fft(IinT,N))/N;
IoutF  = fftshift(fft(IoutT,N))/N;
FElec     = (0:N/2-1)*fsMHz/N;

% This gives the RMS power: multiply by 2 for two sided
% spectrum, square it, then divide by 2 for RMS
% The DC power should not be multiplied by 2.
PinF      = 2*Rohm*abs(IinF(N/2+1:end)).^2;
PoutF     = 2*Rohm*abs(IoutF(N/2+1:end)).^2;
PinF(1)   = PinF(1)/2; PoutF(1) = PoutF(1)/2;

PinFdBm   = 10*log10(PinF) + 30;
PoutFdBm  = 10*log10(PoutF) + 30;

%% Analysis %%

% Calculate the output power for each original tone in dBm
PoutdBm = zeros(1, length(fcMHz));
for x = 1:length(fcMHz)
    PoutdBm(x) = PoutFdBm(find(FElec == fcMHz(x)));
```

```
end

% Calculate the output power at other specified frequencies in dBm
PmondBm = zeros(1, length(monMHz));
for x = 1:length(monMHz)
    PmondBm(x) = PoutFdBm(find(FElec == monMHz(x)));
end

% Function output
output = [PoutdBm, PmondBm];
```

A.2 Small signal simulation of an FM link

The small signal model for an FM link is based on the expression in (2.1.10). It does not include the effects of residual intensity modulation, but includes the effect of the common-mode rejection ratio.

```
function output = model_smsig(param, HaF, HbF, K, fcMHz, PindBm, CMRR)
%MODEL_SMSIG   Small signal model for a frequency modulated link
%   Input param = [fsMHz, N, etaMHz, G, PmW, R, Rohm];
%   Input Ha, Hb are the filter transfer functions, over the range of
%       frequency offsets   f = (-N/2:N/2-1)*fsMHz/N;
%   Input K is the optical power split [Pa/P Pb/P] between the two filters
%   Input fcMHz are the modulation frequencies in MHz [f1, f2, ...]
%   Input PindBm are the modulation powers in dBm [P1, P2, ...]
%   Input CMRR is the common mode rejection ratio for balanced detection
%       in positive decibels. Matlab accepts 'Inf' for perfect CMRR.
%   Output is power [P1, P2, ...] in dBm at frequencies
%       [f1, f2, .... fn, 2*f1, 2*f2, ... 2*fn, 2*f1-f2, 2*f2-f1]

%% Modulation %%
```

```
fsMHz    = param(1); % FFT sampling frequency
N        = param(2); % FFT number of points
etaMHz   = param(3); % Frequency modulation efficiency in MHz/mA
G        = param(4); % RIM normalization parameter
PmW      = param(5); % Optical power before the filters
R        = param(6); % Responsivity of photodetectors
Rohm     = param(7); % Input and output load impedance

% Calculations for modulation
PinW  = 10.^((PindBm-30)/10);   % Input RMS power at each tone in Watts
IA    = sqrt(2*PinW/Rohm);      % Input peak current in Amps
ImA   = IA*1000;                % Peak amplitudes for each tone in mA
df    = etaMHz*ImA;             % Frequency modulation depths
b     = df./fcMHz;              % Phase modulation depths
m     = G*b*2;                  % Intensity modulation depths
PoptW = PmW/1000;               % Optical power in W

% Normalize frequencies
NormF = vectorize(inline('f*N/fsMHz + N/2+1', 'f', 'fsMHz', 'N'));

% Calculate the output power for each original tone in dBm
n = 1; X1a = 0; X1b = 0;
for g = 0:n
    X1a = X1a + (-1)^g/factorial(n-g)/factorial(g).* ...
        HaF(NormF((n-g)*fcMHz,fsMHz,N)).* ...
        conj(HaF(NormF(-g*fcMHz,fsMHz,N)));
    X1b = X1b + (-1)^g/factorial(n-g)/factorial(g).* ...
        HbF(NormF((n-g)*fcMHz,fsMHz,N)).* ...
        conj(HbF(NormF(-g*fcMHz,fsMHz,N)));
end
X1      = X1a*K(1) - X1b*K(2) + (X1a*K(1) + X1b*K(2))*10^(-CMRR./10);
Pout    = 2/(2^(2*n))*Rohm*R^2*PoptW.^2.*b.^(2*n).*abs(X1).^2;
PoutdBm = 10*log10(Pout) + 30;
```

```
% Calculate the output power for the second harmonics in dBm
n = 2; X2a = 0; X2b = 0;
for g = 0:n
    X2a = X2a + (-1)^g/factorial(n-g)/factorial(g).* ...
        HaF(NormF((n-g)*fcMHz,fsMHz,N)).* ...
        conj(HaF(NormF(-g*fcMHz,fsMHz,N)));
    X2b = X2b + (-1)^g/factorial(n-g)/factorial(g).* ...
        HbF(NormF((n-g)*fcMHz,fsMHz,N)).* ...
        conj(HbF(NormF(-g*fcMHz,fsMHz,N)));
end
X2       = X2a*K(1) - X2b*K(2) + (X2a*K(1) + X2b*K(2))*10^(-CMRR./10);
Pout2    = 2/(2^(2*n))*Rohm*R^2*PoptW.^2.*b.^(2*n).*abs(X2).^2;
PoutdBm2 = 10*log10(Pout2) + 30;

% Calculate the output power for the third order distortion in dBm
n = 2; p = 1; X3a = 0; X3b = 0;
fcMHzRR = fcMHz([2 1]); dfRR = df([2 1]);
for g = 0:n
    for k = 0:p
    X3a = X3a + (-1)^(p+g+k)/factorial(n-g)/factorial(g) ...
        /factorial(p-k)/factorial(k).* ...
        HaF(NormF((n-g)*fcMHz+(-p+k)*fcMHzRR,fsMHz,N)).* ...
        conj(HaF(NormF(-g*fcMHz+k*fcMHzRR,fsMHz,N)));
    X3b = X3b + (-1)^(p+g+k)/factorial(n-g)/factorial(g) ...
        /factorial(p-k)/factorial(k).* ...
        HbF(NormF((n-g)*fcMHz+(-p+k)*fcMHzRR,fsMHz,N)).* ...
        conj(HbF(NormF(-g*fcMHz+k*fcMHzRR,fsMHz,N)));
    end
end
X3       = X3a*K(1) - X3b*K(2) + (X3a*K(1) + X3b*K(2))*10^(-CMRR./10);
Pout3    = 2/(2^(2*(n+p)))*Rohm*R^2*PoptW.^2.*...
            b.^(2*n).*(dfRR./fcMHzRR).^(2*p).*abs(X3).^2;
```

```
PoutdBm3 = 10*log10(Pout3) + 30;

% Function output
output = [PoutdBm, PoutdBm2, PoutdBm3];
```

A.3 Large signal simulation of an FM link

The large signal model for an FM link is based on the expression in (2.1.9). It does not include the effects of residual intensity modulation, but includes the effect of the common-mode rejection ratio. Chosing to terminate the infinite series after a large number of terms gives a result with arbitrarily good precision.

```
function output = model_lgsig(param, HaF, HbF, K, fcMHz, PindBm, CMRR)
%MODEL_LGSIG   Large signal model for a frequency modulated link
%   Input param = [fsMHz, N, etaMHz, G, PmW, R, Rohm];
%   Input Ha, Hb are the filter transfer functions, over the range of
%        frequency offsets   f  = (-N/2:N/2-1)*fsMHz/N;
%   Input K is the optical power split [Pa/P Pb/P] between the two filters
%   Input fcMHz are the modulation frequencies in MHz [f1, f2, ...]
%   Input PindBm are the modulation powers in dBm [P1, P2, ...]
%   Input CMRR is the common mode rejection ratio for balanced detection
%        in positive decibels. Matlab accepts 'Inf' for perfect CMRR.
%   Output is power [P1, P2, ...] in dBm at frequencies
%        [f1, f2, .... fn, 2*f1, 2*f2, ... 2*fn, 2*f1-f2, 2*f2-f1]

%% Modulation %%

fsMHz   = param(1); % FFT sampling frequency
N       = param(2); % FFT number of points
etaMHz  = param(3); % Frequency modulation efficiency in MHz/mA
G       = param(4); % RIM normalization parameter
PmW     = param(5); % Optical power before the filters
```

```
R        = param(6); % Responsivity of photodetectors
Rohm     = param(7); % Input and output load impedance

% Calculations for modulation
PinW  = 10.^((PindBm-30)/10);   % Input RMS power at each tone in Watts
IA    = sqrt(2*PinW/Rohm);      % Input peak current in Amps
ImA   = IA*1000;                % Peak amplitudes for each tone in mA
df    = etaMHz*ImA;             % Frequency modulation depths
b     = df./fcMHz;              % Phase modulation depths
m     = G*b*2;                  % Intensity modulation depths
PoptW = PmW/1000;               % Optical power in W

% Normalize frequencies
NormF = vectorize(inline('f*N/fsMHz + N/2+1', 'f', 'fsMHz', 'N'));

% Calculate the output power for each original tone in dBm
n = 1; p = 0; X1a = 0; X1b = 0;
fcMHzRR = fcMHz([2  1]); dfRR = df([2  1]);
for g = -10:11
    for k = -10:11
        X1a = X1a + ...
            besselj(n+g,df./fcMHz).*besselj(k,dfRR./fcMHzRR).* ...
            besselj(g,df./fcMHz).*besselj(k,dfRR./fcMHzRR).* ...
            HaF(NormF((n+g)*fcMHz+k*fcMHzRR,fsMHz,N)).* ...
            conj(HaF(NormF(g*fcMHz+k*fcMHzRR,fsMHz,N)));
        X1b = X1b + ...
            besselj(n+g,df./fcMHz).*besselj(k,dfRR./fcMHzRR).* ...
            besselj(g,df./fcMHz).*besselj(k,dfRR./fcMHzRR).* ...
            HbF(NormF((n+g)*fcMHz+k*fcMHzRR,fsMHz,N)).* ...
            conj(HbF(NormF(g*fcMHz+k*fcMHzRR,fsMHz,N)));
    end
end
X1       = X1a*K(1) - X1b*K(2) + (X1a*K(1) + X1b*K(2))*10^(-CMRR./10);
```

```
Pout     = 2*Rohm*R^2*PoptW.^2.*abs(X1).^2;
PoutdBm = 10*log10(Pout) + 30;

% Calculate the output power for the second harmonics in dBm
n = 2; p = 0; X2a = 0; X2b = 0;
for g = -10:11
    for k = -10:11
        X2a = X2a + ...
            besselj(n+g,df./fcMHz).*besselj(k,dfRR./fcMHzRR).* ...
            besselj(g,df./fcMHz).*besselj(k,dfRR./fcMHzRR).* ...
            HaF(NormF((n+g)*fcMHz+k*fcMHzRR,fsMHz,N)).* ...
            conj(HaF(NormF(g*fcMHz+k*fcMHzRR,fsMHz,N)));
        X2b = X2b + ...
            besselj(n+g,df./fcMHz).*besselj(k,dfRR./fcMHzRR).* ...
            besselj(g,df./fcMHz).*besselj(k,dfRR./fcMHzRR).* ...
            HbF(NormF((n+g)*fcMHz+k*fcMHzRR,fsMHz,N)).* ...
            conj(HbF(NormF(g*fcMHz+k*fcMHzRR,fsMHz,N)));
    end
end
X2       = X2a*K(1) - X2b*K(2) + (X2a*K(1) + X2b*K(2))*10^(-CMRR./10);
Pout2    = 2*Rohm*R^2*PoptW.^2.*abs(X2).^2;
PoutdBm2 = 10*log10(Pout2) + 30;

% Calculate the output power for the third order distortion in dBm
n = 2; p = 1; X3a = 0; X3b = 0;
for g = -10:11
    for k = -10:11
        X3a = X3a + ...
            besselj(n+g,df./fcMHz).*besselj(-p+k,dfRR./fcMHzRR).* ...
            besselj(g,df./fcMHz).*besselj(k,dfRR./fcMHzRR).* ...
            HaF(NormF((n+g)*fcMHz+(-p+k)*fcMHzRR,fsMHz,N)).* ...
            conj(HaF(NormF(g*fcMHz+k*fcMHzRR,fsMHz,N)));
        X3b = X3b + ...
```

```
                besselj(n+g,df./fcMHz).*besselj(-p+k,dfRR./fcMHzRR).*  ...
                besselj(g,df./fcMHz).*besselj(k,dfRR./fcMHzRR).*  ...
                HbF(NormF((n+g)*fcMHz+(-p+k)*fcMHzRR,fsMHz,N)).*  ...
                conj(HbF(NormF(g*fcMHz+k*fcMHzRR,fsMHz,N)));
        end
    end
    X3       = X3a*K(1) - X3b*K(2) + (X3a*K(1) + X3b*K(2))*10^(-CMRR./10);
    Pout3    = 2*Rohm*R^2*PoptW.^2.*abs(X3).^2;
    PoutdBm3 = 10*log10(Pout3) + 30;

    % Function output
    output = [PoutdBm, PoutdBm2, PoutdBm3];
```

Bibliography

[1] J. Capmany and D. Novak, "Microwave photonics combines two worlds," *Nature Photonics*, vol. 1, no. 6, pp. 319–330, Jun 2007. [Online]. Available: http://www.nature.com/doifinder/10.1038/nphoton.2007.89

[2] P. Smyth, "Optical Radio - A Review of a Radical New Technology for Wireless Access Infrastructure," *BT Technology Journal*, vol. 21, pp. 22–31, 2003, 10.1023/A:1025198729319. [Online]. Available: http://dx.doi.org/10.1023/A:1025198729319

[3] S. Pappert, C. Sun, R. Orazi, and T. Weiner, "Microwave fiber optic links for shipboard antenna applications," in *IEEE International Conference on Phased Array Systems and Technology, 2000*, 2000, pp. 345 –348.

[4] K. Y. Lau, *Ultra-high Frequency Linear Fiber Optic Systems*. Springer, 2009.

[5] I. Cox, C.H., E. Ackerman, G. Betts, and J. Prince, "Limits on the performance of RF-over-fiber links and their impact on device design," *Microwave Theory and Techniques, IEEE Transactions on*, vol. 54, no. 2, pp. 906 – 920, Feb 2006.

[6] T. Kakitsuka and S. Matsuo, "High-Speed Frequency Modulated DBR Lasers for Long-Reach Transmission," *IEICE Transactions on Electronics*, vol. E92-C, no. 7, pp. 929–936, Jul 2009.

[7] X. Xie, J. Khurgin, F.-S. Choa, X. Yu, J. Cai, J. Yan, X. Ji, Y. Gu, Y. Fang, Y. Sun, G. Ru, and Z. Chen, "A model for optimization of the performance of frequency-Modulated DFB semiconductor laser," vol. 41, no. 4, pp. 473–482, 2005.

[8] Q. Xiang, Y. Zhao, and F.-S. Choa, "A high-performance RF-lightwave transmitter for analog fiber links," in *Lasers and Electro-Optics Society 2000 Annual Meeting.*, vol. 1, 2000, pp. 138 –139.

[9] J. M. Roth, "Frequency modulated analog fiber optic links using direct detection," Master's thesis, MIT, Cambridge, May 1997.

[10] S. E. Harris, "Demodulation of phase-modulated light using birefringent crystals," *Proceedings of the IEEE*, vol. 52, no. 7, pp. 823 – 831, Jul 1964.

[11] ——, "Conversion of FM Light to AM Light Using Birefringent Crystals," *Applied Physics Letters*, vol. 2, no. 3, p. 47, 1963. [Online]. Available: http://link.aip.org/link/?APL/2/47/1&Agg=doi

[12] S. E. Harris, E. O. Ammann, and I. C. Chang, "Optical Network Synthesis Using Birefringent Crystals. I. Synthesis of Lossless Networks of Equal-Length Crystals," *J. Opt. Soc. Am.*, vol. 54, no. 10, pp. 1267–1278, 1964. [Online]. Available: http://www.opticsinfobase.org/abstract.cfm?URI=josa-54-10-1267

[13] I. P. Kaminow, "Balanced Optical Discriminator," *Applied Optics*, vol. 3, no. 4, p. 507, Apr 1964. [Online]. Available: http://www.opticsinfobase.org/abstract.cfm?URI=ao-3-4-507

[14] S. Saito and T. Kimura, "Demodulation of phase-modulated optical maser beam by autocorrelation technique," *Proceedings of the IEEE*, vol. 52, no. 9, pp. 1048 – 1048, Sep 1964.

[15] S. Kobayashi, Y. Yamamoto, M. Ito, and T. Kimura, "Direct frequency modulation in AlGaAs semiconductor lasers," *IEEE Journal of Quantum Electronics*, vol. 18, no. 4, pp. 582 – 595, Apr 1982.

[16] S. Saito, Y. Yamamoto, and T. Kimura, "Semiconductor laser FSK modulation and optical direct discrimination detection," *Electronics Letters*, vol. 18, no. 11, pp. 468 –469, May 1982.

[17] W. Way, M. Maeda, A. Yi-Yan, M. Andrejco, M. Choy, M. Saifi, and C. Lin, "160-channel FM-video transmission using optical FM/FDM and subcarrier multiplexing and an erbium doped optical fibre amplifier," *Electronics Letters*, vol. 26, no. 2, pp. 139–142, 1990. [Online]. Available: http://link.aip.org/link/?ELL/26/139/1

[18] W. Way, Y. Lo, T. Lee, and C. Lin, "Direct detection of closely spaced optical FM-FDM Gb/s microwave PSK signals," *IEEE Photonics Technology Letters*, vol. 3, no. 2, pp. 176 –178, Feb 1991.

[19] W. V. Sorin, K. W. Chang, G. A. Conrad, and P. R. Hernday, "Frequency domain analysis of an optical FM discriminator," vol. 10, no. 6, pp. 787–793, Jun 1992.

[20] G. Fiksman, R. Gross, J. Fan, and L. Kazovsky, "Performance optimization of directly modulated FM-SCM systems with optical discriminator," *IEEE Photonics Technology Letters*, vol. 5, no. 7, pp. 845 –848, Jul 1993.

[21] V. Urick, F. Bucholtz, P. Devgan, J. McKinney, and K. Williams, "Phase Modulation With Interferometric Detection as an Alternative to Intensity Modulation With Direct Detection for Analog-Photonic Links," *Microwave Theory and Techniques, IEEE Transactions on*, vol. 55, no. 9, pp. 1978 –1985, Sep 2007.

[22] S. Woodward, "Lightwave CATV systems using frequency-modulated laser and interferometer," *Electronics Letters*, vol. 25, no. 24, pp. 1665 –1666, Nov 1989.

[23] G. Yabre and J. Le Bihan, "Intensity modulation technique using a directly frequency-modulated semiconductor laser and an interferometer," *Lightwave Technology, Journal of*, vol. 13, no. 10, pp. 2093 –2098, Oct 1995.

[24] K. Tsukamoto, S. Fujii, P. Sanjo, and S. Komaki, "Theoretical Consideration On Nonlinear Distortion Suppression In Directly Optical FM Microwave over Fiber System," in *International Topical Meeting on Microwave Photonics*, Sep 1997, pp. 251 –255.

[25] J. Chen and R. Brown, "Novel optical frequency discriminator with "perfect" linearity," in *Optical Fiber Communication Conference*, vol. 2, 2000, pp. 329 –331.

[26] X. Xie, J. Khurgin, J. Kang, and F. Choa, "Compact linearized optical FM discriminator," *IEEE Photonic. Tech. L.*, vol. 14, no. 3, pp. 384–386, Mar 2002. [Online]. Available: http://ieeexplore.ieee.org/lpdocs/epic03/wrapper.htm?arnumber=986821

[27] X. Xie, J. Khurgin, J. Kang, and F.-S. Choa, "Ring-assisted frequency discriminator with improved linearity," *IEEE Photonics Technology Letters*, vol. 14, no. 8, pp. 1136–1138, Aug 2002. [Online]. Available: http://ieeexplore.ieee.org/lpdocs/epic03/wrapper.htm?arnumber=1021994

[28] G. Chen, J. Kang, and J. Khurgin, "Frequency discriminator based on ring-assisted fiber sagnac filter," *IEEE Photonics Technology Letters*, vol. 17, no. 1, pp. 109–111, Jan 2005. [Online]. Available: http://ieeexplore.ieee.org/lpdocs/epic03/wrapper.htm?arnumber=1372599

[29] T. Darcie, J. Zhang, P. Driessen, and J. Eun, "Demonstration of a class-B microwave-photonic link using optical frequency modulation and complementary

fiber-Bragg-grating discriminators," in *Optical Fiber Communication Conference*, Mar 2006, pp. 1 – 3.

[30] J. Zhang and T. Darcie, "Low-biased microwave-photonic link using optical frequency or phase modulation and fiber-Bragg-grating discriminator," in *Optical Fiber Communication and the National Fiber Optic Engineers Conference*, Mar 2006, p. 3 pp.

[31] ——, "Clipping-Free Dynamic Range: the Fundamental Limit for Class-B Microwave-Photonic Links," in *International Topical Meeting on Microwave Photonics*, Oct 2006, pp. 1 –4.

[32] T. Darcie, J. Zhang, P. Driessen, and J.-J. Eun, "Class-B Microwave-Photonic Link Using Optical Frequency Modulation and Linear Frequency Discriminators," *IEEE/OSA Journal of Lightwave Technology*, vol. 25, no. 1, pp. 157 –164, Jan 2007.

[33] J. Zhang, A. Hone, and T. Darcie, "Limitation Due to Signal-Clipping in Linearized Microwave-Photonic Links," *IEEE Photonics Technology Letters*, vol. 19, no. 14, pp. 1033 –1035, Jul 2007.

[34] P. Driessen, T. Darcie, and J. Zhang, "Analysis of a Class-B Microwave-Photonic Link Using Optical Frequency Modulation," vol. 26, no. 15, pp. 2740 –2747, Aug 2008.

[35] J. Zhang and T. Darcie, "Two-Tone Analysis of Distortion Suppression in Microwave-Photonic Links Using Phase Modulation and Fiber-Bragg Grating Filters," in *International Symposium on Signals, Systems and Electronics*, Jul 2007, pp. 621 –624.

[36] J. Zhang, T. Darcie, and J. J. Eun, "High-Performance Passive Microwave-Photonic Link for Antenna Remoting Using Truncated Single-Sideband Optical

Phase Detection," in *Optical Fiber Communication and the National Fiber Optic Engineers Conference*, Mar 2007, pp. 1 –3.

[37] J. M. Wyrwas and M. C. Wu, "Dynamic Range of Frequency Modulated Direct-Detection Analog Fiber Optic Links," vol. 27, no. 24, pp. 5552–5562, 2009. [Online]. Available: http://jlt.osa.org/abstract.cfm?URI=JLT-27-24-5552

[38] R. F. Kalman, J. C. Fan, and L. G. Kazovsky, "Dynamic range of coherent analog fiber-optic links," vol. 12, no. 7, pp. 1263–1277, 1994.

[39] C. K. Madsen and J. H. Zhao, *Optical Filter Design and Analysis.* John Wiley & Sons, Inc., 1999.

[40] J. M. Wyrwas and M. C. Wu, "High Dynamic-Range Microwave Photonic Links Using Maximally Linear FIR Optical Filters," in *Optical Fiber Communication Conference.* Optical Society of America, 2010, p. JWA43. [Online]. Available: http://www.opticsinfobase.org/abstract.cfm?URI=OFC-2010-JWA43

[41] K. Takiguchi, K. Jinguji, K. Okamoto, and Y. Ohmori, "Variable group-delay dispersion equalizer using lattice-form programmable optical filter on planar lightwave circuit," *IEEE Journal of Selected Topics in Quantum Electronics*, vol. 2, no. 2, pp. 270 –276, Jun 1996.

[42] K. Takiguchi, S. Kawanishi, H. Takara, A. Himeno, and K. Hattori, "Dispersion slope equalizer for dispersion shifted fiber using a lattice-form programmable optical filter on a planar lightwave circuit," vol. 16, no. 9, pp. 1647 –1656, Sep 1998.

[43] K. Takiguchi, K. Okamoto, and T. Goh, "Planar lightwave circuit dispersion equaliser with reduced bias electrical power employing phase trimming technique," *Electronics Letters*, vol. 36, no. 7, pp. 657–658, 2000. [Online]. Available: http://link.aip.org/link/?ELL/36/657/1

[44] ——, "Integrated optic dispersion slope equaliser for N x 20 Gbit/s WDM transmission," *Electronics Letters*, vol. 37, no. 11, pp. 701–703, 2001. [Online]. Available: http://link.aip.org/link/?ELL/37/701/1

[45] K. Takiguchi, K. Okamoto, T. Goh, and M. Itoh, "Integrated-Optic Dispersion Slope Equalizer for N x Several Tens of Gb/s WDM Transmission," vol. 21, no. 11, p. 2463, 2003. [Online]. Available: http://jlt.osa.org/abstract.cfm?URI=JLT-21-11-2463

[46] K. Takiguchi, H. Takahashi, and T. Shibata, "Tunable chromatic dispersion and dispersion slope compensator using a planar lightwave circuit lattice-form filter," *Optics Letters*, vol. 33, no. 11, pp. 1243–1245, 2008. [Online]. Available: http://ol.osa.org/abstract.cfm?URI=ol-33-11-1243

[47] G.-L. Bona, R. Germann, and B. J. Offrein, "SiON high-refractive-index waveguide and planar lightwave circuits," *IBM Journal of Research and Development*, vol. 47, no. 2.3, pp. 239 –249, Mar 2003.

[48] M. Bohn and C. Xia, "Electrical and optical equalization strategies in direct detected high-speed transmission systems," *AEU - International Journal of Electronics and Communications*, vol. 63, pp. 526 – 532, 2009. [Online]. Available: http://www.sciencedirect.com/science/article/B7GWW-4WD115T-1/2/1399a6fa79891bafae321ff2c9d0d92d

[49] B. Offrein, F. Horst, G. Bona, R. Germann, H. Salemink, and R. Beyeler, "Adaptive gain equalizer in high-index-contrast SiON technology," *IEEE Photonics Technology Letters*, vol. 12, no. 5, pp. 504 –506, May 2000.

[50] M. Bohn, W. Rosenkranz, and P. Krummrich, "Adaptive distortion compensation with integrated optical finite impulse response filters in high bitrate optical com-

munication systems," *IEEE Journal of Selected Topics in Quantum Electronics*, vol. 10, no. 2, pp. 273 – 280, Mar 2004.

[51] M. Bohn and W. Rosenkranz, "Experimental verification of combined adaptive PMD and GVD compensation in a 40 Gb/s transmission using integrated optical FIR-filters and spectrum monitoring," in *Optical Fiber Communication Conference*, vol. 1, Feb 2004, p. 2 vol. (1800).

[52] M. Bohn, P. Krurnmrich, and W. Rosenkranz, "Automatic control of optical equalizers," in *Optical Fiber Communication Conference*, vol. 3, Mar 2005, p. 3 pp. Vol. 3.

[53] M. Bohn, G. Mohs, C. Scheerer, C. Glingener, C. Wree, and W. Rosenkranz, "An adaptive optical equalizer concept for single channel distortion compensation," in *27th European Conference on Optical Communication*, vol. 1, 2001, pp. 6 – 7 vol.1.

[54] M. Bohn, W. Rosenkranz, and G. Mohs, "Multispan inline and adaptive group delay ripple equalization concepts @ 40 Gb/s with optical FIR-filters," in *Optical Fiber Communication Conference*, mar. 2002, pp. 665 – 667.

[55] F. Horst, R. Germann, U. Bapst, D. Wiesmann, B. Offrein, and G. Bona, "Compact tunable FIR dispersion compensator in SiON technology," *IEEE Photonics Technology Letters*, vol. 15, no. 11, pp. 1570 –1572, Nov 2003.

[56] M. Secondini, E. Forestieri, and G. Prati, "Performance of MSE configured PLC optical equalizers for chromatic dispersion compensation," *IEEE Photonics Technology Letters*, vol. 15, no. 2, pp. 248 –250, Feb 2003.

[57] ——, "Adaptive minimum MSE controlled PLC optical equalizer for chromatic dispersion compensation," vol. 21, no. 10, pp. 2322 – 2331, Oct 2003.

[58] ——, "PLC optical equalizer for chromatic and polarization-mode dispersion compensation based on MSE control," *IEEE Photonics Technology Letters*, vol. 16, no. 4, pp. 1173 –1175, Apr 2004.

[59] K. Takiguchi, S. Suzuki, and T. Shibata, "Method for adjusting lattice-form optical devices and its use in realising low-loss variable chromatic dispersion compensator," *Electronics Letters*, vol. 39, no. 4, pp. 355 – 356, Feb 2003.